A Comprehensive Analysis of *Swift*/XRT Data: IV. Single Power-Law Decaying Lightcurves vs. Canonical Lightcurves and Implications for a Unified Origin of X-rays

En-Wei Liang[1], Hou-Jun Lü [1], Shu-Jin Hou[1], Bin-Bin Zhang[2], and Bing Zhang[2]

ABSTRACT

By systematically analyzing the *Swift*/XRT lightcurves detected before 2009 July, we find 19 lightcurves that monotonously decay as a single power law (SPL) with an index of $1 \sim 1.7$ from tens (or hundreds) of seconds to $\sim 10^5$ seconds post the GRB trigger. They are apparently different from the canonical lightcurves characterized by a shallow-to-normal decay transition. We compare the observations of the prompt gamma-rays and the X-rays for these two samples of GRBs (SPL vs. canonical). No statistical difference is found in the prompt gamma-ray properties for the two samples. The X-ray properties of the two samples are also similar, although the SPL sample tend to have a slightly lower neutral hydrogen absorption column for the host galaxies and a slightly larger energy release compared with the canonical sample. The SPL XRT lightcurves in the burst frame gradually merge into a conflux, and their luminosities at 10^5 seconds are normally distributed at $\log L/\mathrm{ergs\ s^{-1}} = 45.6 \pm 0.5$. The normal decay segment of the canonical XRT lightcurves has the same feature. Similar to the normal decay segment, the SPL lightcurves satisfy the closure relations and therefore can be roughly explained with external shock models. In the scenario that the X-rays are the afterglows of the GRB fireball, our results indicate that the shallow decay would be due to energy injection into the fireball and the total energy budget after injection for both samples of GRBs is comparable. More intriguing, we find that a prior X-ray emission model proposed by Yamazaki is more straightforward to interpret the observed XRT data. We show that the zero times (T_0) of the X-rays are $10^2 \sim 10^5$ seconds prior to the GRB trigger for the canonical sample, and satisfy a log-normal distribution. The negligible T_0's of the SPL sample are consistent with being the tail of T_0 distributions at low end, suggesting that the SPL sample and the canonical sample may be from a same parent sample.

[1]Department of Physics, Guangxi University, Nanning 530004, China; lew@gxu.edu.cn

[2]Department of Physics and Astronomy, University of Nevada, Las Vegas, NV 89154; zhang@physics.unlv.edu

Referenced to T_0, the canonical XRT lightcurves well trace the SPL lightcurves. The T_0's of the canonical lightcurves in our analysis are usually much larger than the offsets of the known precursors from the main GRBs. If the prior emission hypothesis is real, the X-ray emission is better interpreted within the external shock models based on the spectral and temporal indices of the X-rays. The lack of detection of a jet-like break in most XRT lightcurves implies that the opening angle of the prior emission jet would be usually large.

Subject headings: radiation mechanisms: non-thermal: gamma-rays: bursts

1. Introduction

Swift, a multi-wavelength gamma-ray burst (GRB) mission (Gehrels et al 2004) has led to great progress in understanding the nature of this phenomenon (Zhang 2007). With the promptly slewing capability, the on-board X-ray Telescope (XRT, Burrows et al. 2004) catches the very early X-rays following the prompt gamma-rays. The X-ray observations led to the identification of a canonical X-ray light curve, which is composed of four successive segments, i.e. an initial steep decay segment (with a decay slope[1] $\alpha_1 > 2$), a shallow decay segment ($\alpha_2 < 0.75$), a normal decay ($\alpha_3 \sim 1$) and a jet-like decay segment ($\alpha_4 > 1.5$) (Tagliaferri et al. 2005; Zhang et al. 2006; Nousek et al. 2006; O'Brien et al. 2006). The lightcurves are usually superimposed by erratic flares (Burrows et al. 2005; Chincarini et al. 2007; Falcone et al. 2007), which may be produced by late activities of the GRB central engine (Burrows et al. 2005; Zhang et al. 2006; Fan & Wei 2005; King et al. 2005; Dai et al. 2006; Perna et al. 2006; Proga & Zhang 2006). The initial steep decay segment is generally believed to be the delayed photons from the high latitudes with respect to the line of sight upon the abrupt cessation of emission in the prompt emission region (Fenimore et al. 1996; Kumar & Panaitescu 2000; Dermer 2004; Dyks et al. 2005; Zhang et al. 2006; Liang et al. 2006; Yamazaki et al. 2006; Nousek et al. 2006; Panaitescu et al. 2006a; Lazzati & Begelman 2006; Zhang et al. 2007a, 2009a; Qin 2009; but see Pe'er et al. 2006, Duran & Kumar, 2009). The origin of the jet-like steep-decay segment occasionally found in a few cases (Burrows & Racusin 2006; Liang et al. 2008; Racusin et al. 2009) is not fully understood. They may be jet breaks, but the chromatic behavior observed in some GRBs posts the issue regarding whether the observed X-ray and optical emissions share the same origin (e.g. Panaitescu et al. 2006b; Liang et al. 2008).

[1]Throughout the paper the notation $f_\nu(t) \propto t^{-\alpha}\nu^{-\beta}$ is adopted

The shallow decay (or plateau) segment is usually seen in the XRT lightcurves (O'Brien et al. 2006a; Liang et al. 2007). The mechanism of this segment is highly debated. Phenomenally, the canonical lightcurves can be well fitted with a two-component model, i.e., a prompt emission component and an afterglow component (Willingale et al. 2007; Ghisellini et al. 2008). The physical origin of the specific function form proposed by Willingale et al. is, however, not understood. The widely discussed model for the shallow decay component is energy injection into the external forward shock either from an long lasting central engine or from an ejecta with a wide distribution of Lorentz factors (Zhang et al. 2006; Nousek et al. 2006; Panaitescu et al. 2006a). Such a picture is supported by the fact that the spectral index does not change across the break and that the segment after the break (normal decay segment) is consistent with the closure relation of the forward shock model (Liang et al. 2007). Although some breaks are consistent with being achromatic, some others show chromatic behavior across the break (Panaitescu et al. 2006b; Liang et al. 2007), suggesting that this model cannot interpret all the data. Liang et al. (2007) argued that the physical origin of the shallow decay segment may be diverse and those plateaus that are followed by abrupt cutoffs might be of internal origin (see also Troja et al. 2007). Ideas going far beyond the traditional fireball models were also proposed. Ioka et al. (2006) argued that there might be a weak prior emission before the GRB trigger, which modified the medium density profile to produce the shallow decay phase. Shao & Dai (2007) interpreted the X-ray lightcurve as due to dust scattering of some prompt X-rays. The model however predicts an evolution of the spectral indices which is not observed in most afterglows (Shen et al. 2008). The upscattering of the forward shock photons by a trailing leptonic shell may also give an X-ray plateau (Panaitescu 2007), but the model is more suitable to interpret X-ray plateaus with sharp cutoffs at the end. Uhm & Beloborodov (2007) and Genet, Daigne & Mochkovitch (2007) suggested that both X-ray and optical afterglows are from a long-lived reverse shock. Ghisellini et al. (2007) argued that the X-ray afterglows is produced by late internal shocks, and the shallow-to-normal transition is due to the jet effect in the prompt ejecta (see also Nava et al. 2007). Kumar et al. (2008) proposed that the observed X-rays are directly related to the accretion power from the central engine, and that the different power law segments in the canonical lightcurves may be related to mass-accretion of different layers of the progenitor stars. Most recently, Yamazaki (2009) suggested that the X-ray emission is prior to the GRB trigger, which may be powered by an earlier activity of the central engine. It may decay with a single power law, but because the offset of the zero time point T_0, the log-log lightcurve with the GRB trigger time as T_0 would display an artificial shallow-to-normal decay transition. This model can interpret no spectral change across the break, and also the chromatic behavior between X-ray and optical, if the optical emission is powered by the ejecta launched during the prompt emission. If correct, it would imply that the GRB activity may start before the gamma-ray trigger.

It is interesting that the XRT lightcurves of a small fraction of *Swift* GRBs monotonously decay with a single power-law (SPL), such as GRB 061007 (Schady et al. 2007). They are apparently different from the majority of bursts that show the canonical lightcurves. This raises the issue about what factors make the difference between the two groups of the XRT lightcurves. Are they really physically different or just due to an uncovered artificial effect? We focus on this issue in this paper by systematically comparing the properties of both the prompt gamma-ray and the X-ray emission properties of these two groups of GRBs. The XRT data reduction, temporal and spectral anlysises, and sample selection are presented in §2. We compare the observations of both the prompt gamma-rays and the X-rays in the shallow-to-normal decay segment between the two groups of GRBs in §3 and §4, respectively. We discuss possible implications from the results of our analysis in §5, and present the conclusions in §6. A concordance cosmology with parameters $H_0 = 71$ km s^{-1} Mpc^{-1}, $\Omega_M = 0.30$, and $\Omega_\Lambda = 0.70$ are adopted.

2. DATA REDUCTION AND SAMPLE SELECTION

The XRT data are downloaded from the *Swift* data archive. We developed a script to automatically download and maintain all the XRT data. The HEAsoft packages, including Xspec, Xselect, Ximage, and *Swift* data analysis tools, are used for the data reduction. We have developed an IDL code to automatically process the XRT data for a given burst in any user-specified time interval. The details of our code have been presented in Zhang et al. (2007a; Paper I) and Liang et al. (2007, 2008; Papers II and III). Our procedure is briefly described as follows.

Our code first runs the XRT tool xrtpipeline to reproduce the XRT clean event data, and then makes pile-up corrections with the same methods as discussed in Romano et al. (2006) (for the Window Timing [WT] mode data) and Vaughan et al. (2006) (for the Photon Counting [PC] mode data). Both the source and background regions are annuli (for PC) or rectangular annuli (for WT). The inner radius of the (rectangular) annuli are dynamically determined by adjusting the inner radius of the annuli through fitting the source brightness profiles with a King (1971) point spread function (for PC) or determined by the photon flux using the method described in Romano et al 2006 (for WT). If the pipe-up effect is not significant, the source regions are in the shape of a circle with radius $R = 20$ pixels (for PC) or of a 40×20 pixels rectangle (for WT) centered at the bursts positions. The background regions have the same size as the source region, but has a distance of 20 pixels away from the source regions. The exposure correction is also made with an exposure map created by XRT tools xrtexpomap. By considering these corrections, the code extracts the background-

subtracted light curve and spectrum for the whole XRT data set. The signal-to-noise ratio for the lightcurves is normally taken as $> 3\sigma$, and it is flexibly adjusted depending on the source brightness.

The XRT data observed from January 2005 to July 2009 for ~ 400 GRBs are reduced with our code. We consider only long duration GRBs (or Type II GRBs; Zhang 2006; Zhang et al. 2007b, 2009b). By visually going through the XRT lightcurves for these bursts, we select those lightcurves that monotonously decay with a SPL from tens or one hundred seconds to $\sim 10^5$ seconds post the GRB triggers without a significant shallow-to-normal segment transition. Only 19 solid cases are identified in our sample. Twelve out of the 19 GRBs have redshift measurements[2]. By removing the superimposed flares from the lightcurves, we fit the lightcurves with a SPL. The lightcurves with our fits are shown in Fig. 1, and the power law indices are reported in Table 1. We perform a time-resolved spectral analysis for the data with an absorbed power-law model, i.e., abs×zabs×power-law, where abs and zabs are the absorbtion models for the Milky Way Galaxy and the GRB host galaxy, respectively, if the redshift of the GRB is available. For a given GRB, we do not consider the evolution of host galaxy $N_H^{\rm host}$, and fix it as the value derived from the fit to the time-integrated spectrum. The values of Γ_X and $N_H^{\rm host}$ derived from the fits to the time-integrated spectrum are reported in Table 1. The time interval taken for the spectral fitting is dynamically determined by the photons accumulated in this time interval, which is required to obtain a photon index with more than 3σ significance. The time-resolved spectral analysis for each burst is shown in Fig 1. The BAT observations of these bursts are collected from the published papers or GCN reports, and they are summarized also in Table 1.

In order to compare the properties of these GRBs to the GRBs having a canonical XRT lightcurve, we compile a sample of 80 XRT lightcurves that have a well-sampled shallow-to-normal transition feature. The initial steep decay segment is removed from these lightcurves since this segment is generally believed to be the GRB tail emission due to the curvature effect as mentioned above. The redshifts of these bursts are also required in order to derive the properties of these bursts in the burst frame. We do not include GRBs 060522, 060607A, and 070110 in our sample since they abruptly transit to a very steep decay phase and they might have a different physical origin (Liang et al. 2007; Troja et al. 2007; Kumar et al. 2008). GRB 060614 is also not included since it may belong to the category of compact star mergers (Type I GRBs) (Gehrels et al. 2006; Zhang 2006; Zhang et al. 2007b, 2009b). We thus get 44 GRBs with redshift measurement in out canonical sample. The observations for

[2]The redshift of GRB 060512 is uncertain. It is reported as 0.4428 by Bloom et al (2006b) but as 2.1 by Starling et al. (2006). We do not include this GRB in the redshift-known sample.

these bursts are summarized in Table 2.

3. THE CHARACTERISTICS OF THE PROMPT GAMMA-RAYS

The distributions of the photon index ($\Gamma_{\rm BAT}$), burst duration (T_{90}), gamma-ray fluence (S_γ), and isotropic gamma-ray energy ($E_{\rm iso,\gamma}$) of the prompt gamma-rays in the BAT band for both the SPL sample (solid) and the canonical sample (dashed) are shown in Fig. 2. We measure the difference of any pair of distributions with the probability (p_{KS}) of the Kolmogorov-Smirnov test (K-S test). The hypothesis that the two distributions are from the same parent sample is statistically rejected if $p_{\rm KS} < 10^{-4}$, and it is marginally rejected if $10^{-4} < p_{\rm KS} < 0.1$. The $p_{\rm KS} = 1$ indicates that the two samples are identical. The values of $p_{\rm KS}$ are marked in each panel of Fig. 2. It is found that the derived p_{KS} are all greater than 0.1, indicating that there are no statistical differences of these distributions between the two groups of GRBs.

4. THE CHARACTERISTICS OF THE X-RAYS

The distributions of the X-ray spectral index (β_X), $N_H^{\rm host}$, and isotropic X-ray energy ($E_{\rm iso,X}$) in the XRT band for the two groups of GRBs are shown in Fig. 3. The comparison of the correlation between $E_{iso,\gamma}$ and $E_{\rm iso,X}$ is also displayed in Fig. 3. The $E_{\rm iso,X}$ is integrated from T_{90} to 10^5 seconds post the GRB trigger. The $E_{{\rm iso},X}$ of the GRBs with a canonical XRT lightcurve is calculated in the same time interval by extrapolating the shallow decay segment to the time of T_{90} without taking the steep decay segment into account. The values of $p_{\rm KS}$ are also marked in Fig. 3. The p_{KS} for the β_X distributions is 0.13, indicating no statistical difference of β_X between the two groups of GRBs. The distributions of both ${N_H}^{\rm host}$ and $E_{\rm iso,X}$ show slight differences between the two samples, with $p_{KS} \sim 10^{-2}$. The $N_H^{\rm host}$ of the SPL sample tend to have a lower N_H and larger $E_{\rm iso,X}$ than the canonical sample, but the slopes of the $E_{\rm iso,X} - E_{\rm iso,\gamma}$ relations are almost the same for the two samples, as displayed in Fig. 3(d).

We derive the lightcurves in the burst frame for the two groups of GRBs, which are presented with isotropic X-ray luminosity (L) as a function of $t/(1+z)$. They are displayed in Figs. 4(a) and 4(b). It is found that the SPL decay lightcurves merge into a conflux at around one day post the GRB trigger. The distribution of the luminosities at 10^5 seconds is shown in Fig. 5(a), with an average of $\log(L_{10^5{\rm s}}/{\rm ergs\ s^{-2}}) = 45.56 \pm 0.55$. Interestingly, the late X-ray luminosity of the canonical sample also shares the similar feature, with an

average of $\log(L_{10^5\mathrm{s}}/\mathrm{ergs\ s^{-2}}) = 45.21 \pm 0.56$. The K-S test for the comparison of the two samples gives $p_{KS} = 0.10$, indicating that there is no statistical difference between the two distributions.

5. Discussion

As shown above, no statistical difference of the prompt gamma-rays between the two groups of GRBs is found, and their spectral characteristics of the X-rays are also consistent with each other. These results likely suggest that the X-rays observed in the two groups may have the same physical origin, and the apparent shallow decay segment in XRT lightcurves would be due to extrinsic effects. We discuss possible explanations of the X-rays in this section. Although some ideas that go far beyond the traditional fireball models were proposed to explain the shallow-to-normal decay segment(see §1), the most popular model is the traditional long lasting energy injection scenario. On the other hand, motivated by our analysis above, we suspect that the smooth shallow-to-normal segment may be due to the real starting time of this emission component is prior to the GRB trigger time, as suggested by Yamazaki (2009). We will discuss these two scenarios.

5.1. The X-rays as the afterglow component of the prompt GRBs

The standard fireball shocks model (Rees & Mészáros 1992, 1993; Mészáros & Rees 1997; Sari et al. 1998; for reviews, see Zhang & Mészáros 2004; Piran 2005; Mészáros 2006) has been found to successfully explain the sparse broad-band afterglow data in pre-*Swift* era (e.g. Panaitescu & Kumar 2002). In the framework of the model, the GRB central engine powers a relativistic jet that is composed of a series of shells with variable Lorentz factors. Irregular collisions among these shells produce the highly variable prompt gamma-rays. As the fireball is decelerated by the ambient medium, a forward shock propagates into the medium and powers the long-term broad band afterglows (Mészáros & Rees 1997; Sari et al. 1998). The decay of the afterglows with time is expected to be a power law with an index ~ 1.0, which would steepen to $1.5 \sim 2$ with an achromatic break if the fireball is collimated into a conical jet (Rhoads 1999; Sari et al. 1999). The SPL decay behavior of the 19 SPL XRT lightcurves is consistent with the prediction of the models. As shown in Paper II, the normal decay phase in the shallow-to-normal decaying segment is consistent with the closure relations predicted by the forward shock models (Sari et al. 1998; Chevalier & Li 2000; Dai & Cheng 2001; Zhang & Mészáros 2004), favoring the idea that the X-ray afterglow is of the external shock origin, and that the shallow decay segment is due to long-lasting energy

injection. Figure 7 presents the model predictions of the closure relations as compared with the two samples (for the canonical sample data are for the normal decay segment). It is found that most of the GRBs are roughly consistent with the closure relations prior to the jet-break for the constant density (ISM) model, suggesting that these XRT lightcurves might be produced by forward shocks. GRBs 061007 and 080319B are marginally accommodated with the closure relations of the pre-jet-break wind model and the post-jet-break ISM model. This suggests that some GRBs may be in a wind-medium (see also Racusin et al. 2008), or with very narrow jet opening angles (see also Schady et al. 2007). We note again that not all X-ray afterglows can be interpreted within the forward shock model due to the chromatic features observed in X-ray/optical lightcurves of some bursts (Panaitescu et al. 2006; Liang et al. 2007, 2008).

Within the forward shock model, the similar late time luminosity for both SPL and canonical X-ray afterglows suggest that the total afterglow energetics of the two groups of bursts may be comparable. The difference then lies in that the SPL GRBs eject the majority of energy promptly with a narrow distribution of large Lorentz factors, while the canonical GRBs either eject the same amount of energy over a long period of time or over a wide range of Lorentz factor distribution. The prompt gamma-ray efficiencies of the two groups of GRB, on the other hand, have to be different: the canonical GRBs typically have a higher gamma-ray emission efficiency than the SPL ones (Zhang et al. 2007c).

5.2. The X-rays as an independent emission component prior to the prompt gamma-rays

Yamazaki (2009) explained the shallow-to-normal decay behavior of the canonical X-ray lightcurves as due to the zero time effect. In his model, the X-ray emission intrinsically decays with a single power law, with starting time point ($-T_0$, with respect to the GRB trigger time) prior to the trigger of the prompt gamma-rays[3]. The observed shallow-to-normal decaying feature is caused by improper zero time point effect. The T_0 of the observed SPL XRT lightcurves would be close to the GRB trigger time. We test this intriguing possibility by searching for a proper T_0 earlier than the BAT trigger time to make the observed shallow-to-normal decay segment be a single power law segment. The shallow-to-normal segment in

[3]Note that T_0 is the onset of the X-ray emission component, but not the peak time of the X-ray emission (Huang et al. 2002; Liang et al. 2006; Yamazaki 2009).

the XRT lightcurves is well fit with a broken power-law,

$$F = F_0 \left[\left(\frac{t}{t_{\rm b}} \right)^{\omega\alpha_1} + \left(\frac{t}{t_{\rm b}} \right)^{\omega\alpha_2} \right]^{-1/\omega}, \quad (1)$$

where ω describes the sharpness of the break, which is taken as 3 in this analysis (Liang et al. 2007). Since α_2 is less affected by the T_0 effect, we assume that the power-law index of an intrinsic XRT lightcurve is α_2, and search its T_0 by fitting the observed shallow-to-normal segment with

$$F = F_0^{'} \left(\frac{t + T_0}{T_0} \right)^{-\alpha_2}. \quad (2)$$

As an example, we show the XRT lightcurves of GRB 080721 referenced to BAT trigger time and to T_0 in Fig. 4(c), along with the XRT lightcurve of GRB 061007, the most prominent case in the sample of the SPL XRT lightcurves. The distributions of $\log T_0$ and the decay slopes of the X-rays referenced to T_0 are shown in Fig. 8. Both the distributions of $\log T_0$ in the observed frame and in the burst frame are well fitted with a Gaussian function, centering at 3.60 ± 0.55 (1σ) and 2.88 ± 0.79 (1σ). The SPL sample would be those GRBs whose T_0 are close to the BAT trigger time. One might suspect whether the *true* T_0 distribution is bimodal by combining the two groups of GRBs. In our sample, the derived T_0 for the canonical sample is longer than 100 seconds. We thus set an upper limit of 100 seconds for the T_0 of X-rays for the SPL sample. Among ~ 400 *Swift* GRBs with detections of X-ray afterglows, about half have a shallow-to-normal decay pattern in their XRT lightcurves (see also Evans et al. 2009). Eighty ones are well-sampled and are selected for our analysis. Considering this sample as a representative one of the canonical sample, a probability of 5% for $T_0 < 100$ is inferred from the derived T_0 distribution of the 80 GRBs, roughly consistent with the percentage of the SPL GRBs in the current Swift GRB sample, i.e., 19/400. Therefore, the current data is consistent with the hypothesis that SPL GRBs are from the same parent sample as the canonical ones, but belong to the lower end of the $\log T_0$ distribution derived from the canonical sample.

The T_0 is the time interval between the starting time of the X-ray emission and that of the prompt gamma-ray emission. It is worth investigating if there are any correlations between T_0 and some observables of the prompt gamma-rays. We find that T_0 is not correlated with T_{90}, but it is tentatively anti-correlated with the isotropic gamma-ray peak luminosity (or isotropic gamma-ray energy) and the photon index of the prompt gamma-rays. As shown in Fig. 6, a $L_p - T_0/(1+z)$ correlation and a $\Gamma_{\rm BAT} - T_0/(1+z)$ correlation with the Spearman correlation coefficients $r = -0.58$ (chance probability $p < 10^{-4}$) and $r = -0.39$ ($p \sim 10^{-2}$) are derived. This implies that brighter or harder bursts tend to have a shorter time interval between the burst itself and the prior X-ray emission. However, the correlations are not tight, and should be taken with caution.

Precursors at tens or even hundreds of seconds prior to main bursts have been detected in some GRBs (e.g. Lazzati 2005; Burlon et al. 2008). It would be interesting to test whether these precursors are related to the prior emission discussed in this paper. Well-sampled precursors were detected in GRBs 060124 and 061121 in the Swift GRB sample. Their XRT lightcurves also behave as canonical ones. We therefore check their inferred T_0 and consistency with the leading time between the precursor and the main burst. We find that T_0 leads the precursor time significantly. GRB 060124 has a precursor ~ 570 seconds prior to the main burst peak (Romano et al. 2006), but its X-ray T_0 is $(5.57 \pm 0.58) \times 10^3$ seconds before the trigger (precursor), which is $(6.14 \pm 0.58) \times 10^3$ seconds before the main burst. The precursor of GRB 061121 is at ~ 60 seconds prior to the main burst(Page et al. 2007), but its X-rays T_0 is $(3.09 \pm 0.08) \times 10^3$ seconds prior to the GRB trigger (precursor) and $(3.15 \pm 0.08) \times 10^3$ seconds before the main burst. This seems to suggest that the prior emission is another component other than the precursor. However, we emphasize that T_0 is the beginning of the prior emission component, not necessarily the peak of the prior emission, which is expected to be later from T_0 and closer to the GRB main peak. The possibility that the precursor is related to the prior emission is not ruled out. Since the T_0's derived in this paper are all with respect to the BAT trigger time, it may pick up some precursors rather than the main bursts as the reference point. This would bring confusions to the measured T_0 and contribute the scatter of the correlations presented in Fig. 6.

In general, the T_0 effect is a major issue of presenting lightcurves in the log-log space. Shifting T_0 can effectively modify the power-law decay indices of a lightcurve, which directly affect the theoretical interpretation of the phenomena. Recalling the history of the GRB study, we caution that T_0 is a two-edged weapon that can be used equally for good or bad. Moving T_0 after the GRB trigger time, Liang et al. (2006) found that the early steep decay segment of the XRT lightcurves can be explained by the tail emission of the last emission epoch, and that X-ray flares are consistent with being late internal emission related to the central engine. On the other hand, by setting T_0 to near the X-ray flares, Piro et al. (2005) found that the X-ray flares in GRBs 011121 and 011211 are consistent with the onsets of the X-ray afterglows, and hence, missed to report the first detections of flares in GRBs[4]. Here, by putting T_0 prior to the GRB trigger time, we argue that a shallow-to-normal decay

[4]Note that X-ray flares are likely related to reactivation of the central engine at later times. time should be set to before the onset of the X-ray flares (Liang et al. 2006). They are an independent component superimposed onto the underlying prior X-ray emission component. Phenomenologically, if one plots X-ray afterglow lightcurve with respect to T_0, then early X-ray flares (occurring at epochs shorter than T_0 after the trigger time) would appear "narrower", i.e., having steeper rising and falling indices. The late X-ray flares (those occurring at epochs longer than T_0 after the trigger time) would look similar to the ones plotted referencing the trigger time.

segment can become a single power-law (Yamazaki 2009). Such a suggestion may be at risk. However, since it is an intriguing possibility and can be tested by future observations, in the following we will explore the consequence of such an assumption. We will investigate whether moving T_0 would make a better consistency between the canonical and the SPL samples.

All XRT lightcurves referenced to T_0 are shown in Fig. 4(d) along with the observed SPL XRT lightcurves. It is interesting that they well trace the observed SPL XRT lightcurves. The distributions of the X-ray luminosity at $t = 10^2$, 10^3, and 10^5 seconds referenced to T_0 ($L_{X,t}^{T_0}$) and to the BAT trigger time ($L_{X,t}^{\rm BAT}$) are shown in Fig. 5, with comparisons to the SPL GRBs[5]. It is found that $\log L_{X,10^2s}^{\rm BAT}$ falls in the range of [46, 50] with an average of $48.1 \pm 0.9(1\sigma)$, and $\log L_{X,10^2s}^{\rm T_0}$ in the range of [47, 52] with an average of $49.5 \pm 1.0(1\sigma)$, typically being larger than $\log L_{X,10^2s}^{\rm BAT}$ with 1.4 orders of magnitude. For the SPL GRB sample, the $\log L_{X,10^2}^{\rm SPL}$ distribution is in the range of [48, 51] with an average of $49.8 \pm 0.5(1\sigma)$, roughly consistent with $\log L_{X,10^2s}^{\rm T_0}$. We measure the consistency of the luminosity distributions to that of the SPL GRBs by the K-S test, which gives $p_{K-S} = 4.08\times10^{-3}$ and $p_{K-S} = 6.14\times10^{-2}$ for $\log L_{X,10^2s}^{\rm BAT}$ and $\log L_{X,10^2s}^{\rm T_0}$, respectively, indicating that the distribution of $\log L_{X,10^2s}^{\rm T_0}$ is more consistent with that of the SPL GRB sample. The distributions of $L_{X,10^5s}^{\rm BAT}$ and $L_{X,10^5s}^{\rm T_0}$ are consistent with each other, and they also well agree with that of the SPL GRB sample.

In order to compare the X-ray luminosity with the peak luminosity of prompt gamma-ray emission $L_{p,\gamma}$, we show the SPL GRBs (*solid circles*) and canonical GRB samples in the $(L_{X,10^2s} - L_{\gamma,p})$-plane and $(L_{X,10^3s} - L_{\gamma,p})$-plane, where the time of the X-ray luminosity for the canonical samples is referenced to the BAT trigger time or to T_0 in Fig. 9. Comparisons of the distributions of $\log L_X^{BAT}/L_{\gamma,p}$ and $\log L_X^{T_0}/L_{\gamma,p}$ at 10^2 and 10^3 seconds for the canonical sample to the SPL sample are also shown in Fig. 9. Except for seven GRBs, the $L_{X,10^2s}^{\rm T_0}$ of the other GRBs are smaller than $0.1L_{p,\gamma}$, and the $L_{X,10^3s}^{\rm T_0}$ of all GRBs are smaller than $0.1L_{p,\gamma}$. For the seven GRBs, their $L_{X,10^2s}^{\rm T_0}$ are comparable to $L_{p,\gamma}$. It is possible that the peak time of the X-ray emission is at a time later than 100 seconds with respect to T_0, and their $L_{X,10^2s}^{\rm T_0}$ would be over-estimated. Excluding the seven GRBs, more consistency is observed between the two groups of GRBs in the $L_{p,\gamma} - L_X^{T_0}$ planes. Even considering the seven cases, the $L_{X,10^2}^{T_0}$ of the canonical sample is still more consistent with the SPL sample than $L_{X,10^2}^{BAT}$(testing by K-S test, as marked in Fig. 9).

[5]With a sample of 16 pre-*Swift* X-ray afterglow lightcurves, Gendre & Boër (2005) suggested two classes of GRBs defined by the X-ray afterglow luminosity. This signature is possibly related to the two groups of XRT lightcurves discussed in this paper. Although the early X-ray luminosities (at 10^2 second) of the SPL XRT lightcurves tend to be brighter than those of the canonical ones, we do not confirm the bimodal distributions of the X-ray luminosity at 10^3 second and 10^5 second, as shown in Fig.5.

The analysis above indicates that the canonical XRT lightcurves may have the same physical origin as the SPL XRT lightcurves, and the apparent shallow-to-normal segment is due to improper zero time point. The zero time points of those observed single power-law XRT lightcurves are possibly comparable to the BAT trigger time. The fraction of these GRBs is very small in the current *Swift* GRB sample, i.e., 19 cases out of $\sim$ 400 GRBs. The X-rays may be a long-lasting emission component prior to the GRB trigger time as suggested by Yamazaki (2009). The discovery of the X-ray flares following a good fraction of GRBs suggest that a long-live GRB central engine is common for GRBs (Burrows et al. 2005; Zhang et al. 2006; Fan & Wei 2005; King et al. 2005; Dai et al. 2006; Perna et al. 2006; Proga & Zhang 2006). The prior emission requires that the central engine activity time scale is stretched even longer.

In principle, a prior X-ray emission decaying as a single power-law may be originated both from an external shock or central-engine-powered internal dissipation. In the scenario of a central-engine-powered X-ray emission model, the X-rays might be powered by an unknown internal dissipation mechanism, and the X-ray luminosity is conjectured to track the accretion power at the central engine. The accretion rate by the central engine may be expressed by (e.g. Kumar et al. 2008)

$$\dot{M} \sim \dot{M}(t_0)(1+\frac{3}{2s+1}\frac{t-t_0}{t_{acc}})^{-4(s+1)/3}, \quad (3)$$

where t_{acc} is a characteristic timescale of accretion and $0 < s < 1$. The luminosity can be then estimated by $L = \eta \dot{M} c^2$. The observed decay slope of the X-rays is $1 \sim 2$, being roughly consistent with Eq. 3. The parameter s is quite uncertain. As shown in Fig. 4, the decay slopes of the lightcurves are $-4/3 \sim -5/3$. Critical concern on this scenario is that it requires the central engine to be active as long as 10^5 seconds, even 10^7 seconds (e.g., GRB 060729). The strong dependence of the neutrino annihilation mechanism on the mass accretion rate makes it difficult to explain the data (e.g., Barkov & Komissarov 2009). The neutrino mechanism requires the mass accretion rate to stay over few $0.01 M_\odot$/s (e.g., Fan, Zhang & Proga 2005; Popham et al. 1999). Long-lasting accretion implies the progenitor mass is above hundreds of solar mass. However, the mass of a WR star is 9-25 $M_\odot$, though some observations suggested that it can be as high as 83 $M_\odot$(Schweickhardt et al. 1999; Crowther 2007).

A more straightforward model to explain the power-law decay of the X-rays is the external shock model. As shown in Fig. 7, the X-rays are generally consistent with the external shock models, similar to the GRB afterglows. They may be also produced by interaction of an early ejecta launched prior to the formation of the GRB jet with the circumburst medium. The observed flux should increase and then decay as a single power law post the peak of the emission. Within the ISM forward shock model the decay slopes

of the X-rays varies between 0.75 and 1.5, depending on the observed spectral index and medium properties (e.g., paper III). We thus mark $L \propto t^{-0.75}$ and $L \propto t^{-1.5}$ in Fig. 4. It is found that the data are well consistent with the model prediction. Note that the T_0 is the start time of the X-ray emission component, but not its peak time. In the external shock scenario, the peak time of the X-rays can be estimated by (Mészáros & Rees 1993; Sari & Piran 1999)

$$t_p \approx 10^3 (1+z) E_{iso,X,52}^{1/3} \eta_{0.2}^{-1/3} n^{-1/3} \Gamma_{0,2}^{-8/3}, \quad (4)$$

where $E_{iso,X,52} = E_{iso,X}/10^{52}$erg, $\eta_{0.2} = \eta/0.2$ is the radiative efficiency, n is the medium density, and $\Gamma_{0,2} = \Gamma_0/10^2$ is the initial Lorentz factor of the fireball. As shown in Fig. 8(a), the T_0 of the X-rays for most bursts are several thousands of seconds. This suggests that the peak time of the X-rays for some GRBs may be close to the BAT trigger time.

One related question is the jet break in the prior emission. Inspecting the SPL sample (Fig. 1), we find that only GRBs 080413 and 080913B show a jet-like break at $\times 10^5$ seconds, and that the others have no break feature. For the canonical sample, our T_0 search can make the shallow-decay phase to have the same decay slope as the normal decay phase. However, if there is a late jet-like break in the canonical lightcurve, such a break should still exist after the T_0 shift. An example is GRB 060729 (Fig. 4c). In general these breaks tend to be late, too. These facts imply that the prior X-ray emission would be usually from a jet with a large opening angle. Again taking GRB 060729 as an example. The X-ray emission was observed up to 642 days after the GRB trigger and a jet-like break was observed at around 1 year after the GRB trigger (Grupe et al. 2009)[6]. A jet-like break is usually seen in the lightcurves of the optical afterglows at days to one week post the GRB triggers. The jet that is associated with the prompt gamma-ray emission thus might be generally narrower than the jet for the prior X-ray emission, if the optical emission is the afterglows of the jet related to the prompt emission.

6. CONCLUSIONS

By systematically analyzing the XRT lightcurves for $\sim$ 400 *Swift* GRBs detected by June 2009, we have investigated the properties of the GRBs with a SPL decaying XRT lightcurve and made comparisons between these GRBs (the SPL sample) and the GRBs having a canonical XRT lightcurve (the canonical sample). We only find 19 GRBs whose XRT lightcurves decay with a SPL from tens to $\sim 10^5$ seconds post the GRB triggers. The

[6]The steep temporal decay and significant spectral softening after the break also favor a spectral origin for the break(Grupe et al. 2009).

decay slopes of these lightcurves range from $1 - 1.7$. The fraction of these GRBs in the whole *Swift* sample is small, i.e., 19 out of ~ 400, suggesting that the SPL lightcurves are much less common than the canonical ones. There is no statistical difference between the distributions of T_{90}, $E_{iso,\,\gamma}$, and $\Gamma_{\rm BAT}$ of the prompt gamma-ray parameters for the two groups (SPL vs. canonical) of GRBs. No significant spectral evolution is observed for the X-rays with the SPL decay, similar to that observed in the canonical GRBs (Paper II). No statistical difference of the X-ray spectra is found between the two groups of GRBs, and the power-law indices of the $E_{\rm iso,X} - E_{\rm iso,\gamma}$ relations for the two GRB samples are almost the same. However, the SPL sample tends to have a slightly lower neutral hydrogen absorption column by the host galaxy and a slightly larger energy release in the X-ray band than the canonical sample.

The SPL lightcurves in burst frame gradually merge into a conflux at around one day post the GRB trigger. A Gaussian function fit in logarithmic scale to the luminosity distribution at 10^5 s yields $\log(L_{10^5{\rm cm}}/{\rm ergs\ s^{-1}}) = 45.50 \pm 0.70$. The normal decay phase in the shallow-to-normal segment of the canonical GRBs share the similar feature. Confronting the data with the predictions of the external shock models, we find that the SPL lightcurves are generally consistent with the models, similar to the normal decay phase of the canonical lightcurves. The external shock origin of both the SPL lightcurves and the normal decay segments in the canonical XRT lightcurves is favored. If the shallow decay is due to energy injection into the fireball, the total energy budget after injection for both samples of GRBs is similar.

The apparent shallow decay phase in the canonical sample may also be due to the T_0 effect of a SPL X-ray emission component prior to the GRB trigger, as suggested by Yamazaki (2009). By setting the T_0 at an epoch before the GRB trigger, we show that a shallow-to-normal segment becomes a SPL with the same decay index as the normal decay phase. The XRT lightcurves referenced to T_0 also well trace the observed SPL XRT lightcurves. This likely suggests that the X-rays might be a long-lasting emission component starting before the GRB trigger and the SPL sample might be composed of the GRBs whose T_0's are close to the GRB trigger times. Although precursors at tens or even hundreds of seconds prior to main bursts were detected in some GRBs, their spectral properties reveals that the precursors are not a phenomenon distinct from the main event, and the prior time offset of the X-rays in our analysis is much larger than that the offset of the known precursors. However, the peak time of the prior emission is different from T_0, so the possibility that the precursors are related to the prior emission is not ruled out.

As shown above the external shock model invoking an emission component prior to the GRB prompt emission may give a unified picture to interpret the canonical and SPL

XRT lightcurves. In this scenario the GRB phenomenon should invoke two different ejecta components that are responsible for the observed X-ray afterglow and the prompt emission (along with the optical afterglow in most cases), respectively. The mixture of radiation from these two components would bring complication and confusion on the identifications of them. The well-sampled lightcurves of early optical/IR afterglows usually show a smooth onset feature as expected from the deceleration of the GRB fireball for some GRBs, such as GRBs 060418 and 060607A (Molinari et al. 2007), and a jet break is also usually observed in the late optical lightcurves (Sari et al. 1999). These facts suggest that the optical afterglows would be dominated by the external shock of the jet that is associated with the prompt emission. On the other hand, such an early onset feature is not common in XRT lightcurves, only detected in a few GRBs, such as GRB 080307 (Page et al. 2009). This is partially due to the contamination of the X-rays associated with the prompt emission (e.g. the steep decay tail), but is also consistent with the hypothesis of an earlier onset of X-ray afterglow. The deficiency of X-ray jet breaks (Liang et al. 2008; Racusin et al. 2009) is consistent with the hypothetical wider opening angle of the prior jet. The chromatic breaks in the optical and X-ray lightcurves for some GRBs (Papers II and III) demand that the X-ray and optical are two different emission components. The prior emission model requires that the X-rays should be dominated by the prior emission component, while the optical emission (in most cases) is related to the ejecta from the prompt emission. This requires that the X-ray afterglow associated with the prompt emission jet is buried beneath the X-ray emission related to the prior component, while the optical emission of the prior component is outshone by that of the prompt emission component. This is great concern of this model, along with any other models that invoke two emission components (e.g. Ghisellini et al. 2008). Detailed theoretical modeling is called for and is in plan.

We acknowledge the use of the public data from the Swift data archive. We appreciate valuable comments/suggentions from the referee. We also thank helpful discussion with Zi-Gao Dai, Kunihito Ioka, Wei-Hua Lei, Tong Liu, Milhail Medvedev, Paul O'Brien, Rob Preece, Ryo Yamazaki, Ding-Xiong Wang, Xiang-Yu Wang, Jian-Yan Wei, and Shuang-Nan Zhang. This work was supported by the National Natural Science Foundation of China under grants No. 10873002, the National Basic Research Program ("973" Program) of China (Grant 2009CB824800), the research foundation of Guangxi University(M30520), and NASA NNG05GB67G, NNX08AN24G, and NAX08AE57A. BBZ acknowledges the President's Fellow Ship and GPSA awards from UNLV.

REFERENCES

Barkov, M. V., & Komissarov, S. S. 2009, arXiv:0908.0695

Berger, E., et al. 2005, GRB Coordinates Network, 3368, 1

Berger, E., et al. 2008, GRB Coordinates Network, 8335, 1

Bloom, J. S., et al. 2006a, GRB Coordinates Network, 5217, 1

Bloom, J. S., et al. 2006b, GRB Coordinates Network, 5826, 1

Bloom, J. S., et al. 2009, ApJ, 691, 723

Burlon, D., Ghirlanda, G., Ghisellini, G., Lazzati, D., Nava, L., Nardini, M., & Celotti, A. 2008, ApJ, 685, L19

Burrows, D. N., & Racusin, J. 2006, Nuovo Cimento B Serie, 121, 1273

Burrows, D. N., et al. 2004, Proc. SPIE, 5165, 201

Burrows, D. N., et al. 2005, Science, 309, 1833

Cenko, S. B., et al. 2005, GRB Coordinates Network, 3542, 1

Cenko, S. B., et al. 2006, GRB Coordinates Network, 4592, 1

Cenko, S. B., et al. 2009, GRB Coordinates Network, 9518, 1

Chandra, P., & Frail, D. A. 2007, GRB Coordinates Network, 6740, 1

Chen, H.-W., et al. 2007, GRB Coordinates Network, 6217, 1

Chevalier, R. A., & Li, Z.-Y. 2000, ApJ, 536, 195

Chincarini, G. et al. 2007, ApJ, 671, 1903

Chornock, R., et al. 2009, GRB Coordinates Network, 9151, 1

Chornock, R., et al. 2009, GRB Coordinates Network, 9243, 1

Crowther, P. A. 2007, ARA&A, 45, 177

Cucchiara, A., & Fox, D. B. 2008, GRB Coordinates Network, 7290, 1

Cucchiara, A., & Fox, D. B. 2008, GRB Coordinates Network, 7654, 1

Cucchiara, A., et al. 2006, GRB Coordinates Network, 5052, 1

Cucchiara, A., et al. 2008, GRB Coordinates Network, 7615, 1

Cucchiara, A., et al. 2008, GRB Coordinates Network, 8346, 1

Cucchiara, A., et al. 2008, GRB Coordinates Network, 8713, 1

Dai, Z. G., & Cheng, K. S. 2001, ApJ, 558, L109

Dai, Z. G., Wang, X. Y., Wu, X. F., & Zhang, B. 2006, Science, 311, 1127

D'Avanzo, P., et al. 2008, GRB Coordinates Network, 7997, 1

de Ugarte Postigo, A., et al. 2009, GRB Coordinates Network, 8766, 1

de Ugarte Postigo, A., et al. 2009, GRB Coordinates Network, 9383, 1

Dermer, C. D. 2004, ApJ, 614, 284

Dupree, A. K., et al. 2006, GRB Coordinates Network, 4969, 1

Duran, R. B., & Kumar, P. 2009, MNRAS, 395, 955

Dyks, J., Zhang, B., & Fan, Y. Z. 2005, arXiv:astro-ph/0511699

Evans, P. A., et al. 2008, arXiv:0812.3662

Falcone, A. D., et al. 2007, ApJ, 671, 1921

Fan, Y. Z., & Wei, D. M. 2005, MNRAS, 364, L42

Fan, Y. Z., Zhang, B., & Proga, D. 2005, ApJ, 635, L129

Fatkhullin, T. A., et al. 2007, GRB Coordinates Network, 6984, 1

Fenimore, E. E., Madras, C. D., & Nayakshin, S. 1996, ApJ, 473, 998

Fernandez-Soto, A., et al. 2009, GRB Coordinates Network, 9222, 1

Filgas, R., et al. 2008, GRB Coordinates Network, 7747, 1

Fynbo, J. P. U., et al. 2005, GRB Coordinates Network, 3136, 1

Fynbo, J. P. U., et al. 2005, GRB Coordinates Network, 3176, 1

Fynbo, J. P. U., et al. 2005, GRB Coordinates Network, 3749, 1

Fynbo, J. P. U., et al. 2005, GRB Coordinates Network, 3874, 1

Fynbo, J. P. U., et al. 2006, GRB Coordinates Network, 5651, 1

Fynbo, J. P. U., et al. 2008, GRB Coordinates Network, 7949, 1

Gehrels, N., et al. 2004, ApJ, 611, 1005

Gehrels, N., et al. 2006, Nature, 444, 1044

Gendre, B., & Boër, M. 2005, A&A, 430, 465

Genet, F., Daigne, F.,& Mochkovitch, R. 2007, MNRAS, 381, 732

Ghisellini, G., Ghirlanda, G., Nava, L., & Firmani, C. 2007, ApJ, 658, L75

Ghisellini, G., Nardini, M., Ghirlanda, G., & Celotti, A. 2008, arXiv:0811.1038

Grazian, A., et al. 2006, GRB Coordinates Network, 4545, 1

Grupe, D., et al. 2009, arXiv:0903.1258

Hessels, J., et al. 2008, GRB Coordinates Network, 8212, 1

Huang, Y. F., Dai, Z. G., & Lu, T. 2002, MNRAS, 332, 735

Ioka, K., Toma, K., Yamazaki, R., & Nakamura, T. 2006, A&A, 458, 7

Jakobsson, P., et al. 2005, GRB Coordinates Network, 4017, 1

Jakobsson, P., et al. 2006, GRB Coordinates Network, 5320, 1

Jakobsson, P., et al. 2006, GRB Coordinates Network, 5617, 1

Jakobsson, P., et al. 2007, GRBCoordinates Network, 6283, 1

Jakobsson, P., et al. 2007, GRB Coordinates Network, 6398, 1

Jakobsson, P., et al. 2008, GRB Coordinates Network, 7832, 1

Jaunsen, A. O., et al. 2007, GRB Coordinates Network, 6202, 1

King, A., O'Brien, P. T., Goad, M. R., Osborne, J., Olsson, E., & Page, K. 2005, ApJ, 630, L113

King, I. R. 1971, PASP, 83, 199

Kumar, P., & Panaitescu, A. 2000b, ApJ, 541, L51

Kumar, P., Narayan, R., & Johnson, J. L. 2008, Science, 321, 376

Landsman, W., et al. 2008, GRB Coordinates Network, 8601, 1

Lazzati, D. 2005, MNRAS, 357, 722

Lazzati, D., & Begelman, M. C. 2006, ApJ, 641, 972

Liang, E. W., et al. 2006, ApJ, 646, 351

Liang, E.-W., Zhang, B.-B., & Zhang, B. 2007, ApJ, 670, 565

Liang, E.-W., Racusin, J. L., Zhang, B., Zhang, B.-B., & Burrows, D. N. 2008, ApJ, 675, 528

Mészáros, P. 2006, Reports of Progress in Physics, 69, 2259

Malesani, D., et al. 2009, GRB Coordinates Network, 9457, 1

Mészáros, P., & Rees, M. J. 1997, ApJ, 476, 232

Mészáros, P., & Rees, M. J. 1993, ApJ, 405, 278

Molinari, E., et al. 2007, A&A, 469, L13

Nava, L., Ghisellini, G., Ghirlanda, G., Cabrera, J. I., Firmani, C., & Avila-Reese, V. 2007, MNRAS, 377, 1464

Nousek, J. A., et al. 2006, ApJ, 642, 389

O'Brien, P. T., et al. 2006, ApJ, 647, 1213

Osip, D., et al. 2006, GRB Coordinates Network, 5715, 1

Page, K. L., et al. 2007, ApJ, 663, 1125

Page, K. L., et al. 2009, MNRAS, 395, 328

Panaitescu, A., & Kumar, P. 2002, ApJ, 571, 779

Panaitescu, A., Mészáros, P., Gehrels, N., Burrows, D., & Nousek, J. 2006a, MNRAS, 366, 1357

Panaitescu, A et al. 2006b, MNRAS, 369, 2059

Panaitescu, A., Mészáros, P., Burrows, D., Nousek, J., Gehrels, N., O'Brien, P., & Willingale, R. 2006, MNRAS, 369, 2059

Panaitescu, A. 2007, MNRAS, 380, 374

Pe'er, A., Mészáros, P., & Rees, M. J. 2006, ApJ, 652, 482

Perley, D. A., et al. 2007, GRB Coordinates Network, 6850, 1

Perley, D. A., et al. 2008, GRB Coordinates Network, 7962, 1

Perna, R., Armitage, P. J., & Zhang, B. 2006, ApJ, 636, L29

Piran, T. 2005, Reviews of Modern Physics, 76, 1143

Piranomonte, S., et al. 2006, GRB Coordinates Network, 4520, 1

Piro, L., et al. 2005, ApJ, 623, 314

Popham, R., Woosley, S. E., & Fryer, C. 1999, ApJ, 518, 356

Prochaska, J. X., et al. 2008, GRB Coordinates Network, 7388, 1

Proga, D., & Zhang, B. 2006, MNRAS, 370, L61

Qin, Y. -P. 2009, ApJ, 691, 811

Quimby, R., et al. 2005, GRB Coordinates Network, 4221, 1

Racusin, J. L., et al. 2008, Nature, 455, 183

Racusin, J. L., Liang, E. W. Burrows, D. N. Falcone, A. et al. 2009, ApJ, 698, 43

Rees, M. J., & Mészáros, P. 1992, MNRAS, 258, 41

Rhoads, J. E. 1999, ApJ, 525,737

Rol, E., et al. 2006, GRB Coordinates Network, 5555, 1

Romano, P., et al. 2006, A&A, 456, 917

Sari, R., & Piran, T. 1999, ApJ, 520, 641

Sari, R., Piran, T., & Narayan, R. 1998, ApJ, 497, L17

Sari, R., Piran, T., & Halpern, J. P. 1999, ApJ, 519, L17

Schady, P., et al. 2007, MNRAS, 380, 1041

Schweickhardt, J., Schmutz, W., Stahl, O., Szeifert, T., & Wolf, B. 1999, A&A, 347, 127

Shao, L., & Dai, Z. G. 2007, ApJ, 660, 1319

Shen, R.-F., Duran, R. B., & Kumar, P. 2008, MNRAS, 384, 1129

Soderberg, A. M., et al. 2005, GRB Coordinates Network, 4186, 1

Starling, R., et al. 2006, GRB Coordinates Network, 5149, 1

Tagliaferri, G., et al. 2005, Nature, 436, 985

Thoene, C. C., et al. 2006, GRB Coordinates Network, 5373, 1

Thoene, C. C., et al. 2007, GRB Coordinates Network, 6663, 1

Thoene, C. C., et al. 2007, GRB Coordinates Network, 6741, 1

Thoene, C. C., et al. 2008, GRB Coordinates Network, 8058, 1

Troja, E., et al. 2007, ApJ, 665, 599

Uhm, Z. L., & Beloborodov, A. M. 2007, ApJ, 665, L93

Vaughan, S., et al. 2006, ApJ, 638, 920

Vreeswijk, P., et al. 2006, GRB Coordinates Network, 5535, 1

Vreeswijk, P. M., et al. 2008, GRB Coordinates Network, 8191, 1

Willingale, R., et al. 2007, ApJ, 662, 1093

Yamazaki, R., Toma, K., Ioka, K., & Nakamura, T. 2006, MNRAS, 369, 311

Yamazaki, R. 2009, ApJ, 690, L118

Zhang, B. 2006, Nature, 444, 1010

Zhang, B. 2007, Chinese Journal of Astronomy and Astrophysics, 7, 1

Zhang, B., & Mészáros, P. 2004, International Journal of Modern Physics A, 19, 2385

Zhang, B., Fan, Y. Z., Dyks, J., Kobayashi, S., Mészáros, P., Burrows, D. N., Nousek, J. A., & Gehrels, N. 2006, ApJ, 642, 354

Zhang, B., Zhang, B.-B., Liang, E.-W., Gehrels, N., Burrows, D. N., & Mészáros, P. 2007b, ApJ, 655, L25

Zhang, B., Liang, E.-W., Page, K., Grupe, D., et al. 2007c, ApJ, 655, 989

Zhang, B.-B., Liang, E.-W., & Zhang, B. 2007a, ApJ, 666, 1002

Zhang, B.-B., Zhang, B., Liang, E.-W., & Wang, X.-Y. 2009a, ApJ, 690, L10

Zhang, B., Zhang, B.-B., Virgili, F., Liang, E.-W. Kann, D. A. et al. 2009b, ApJ, in press (arXiv:0902.2419)

Table 1. The observations and our fits for the GRBs with a single power law decaying XRT lightcurve

GRB	T_{90}(s)	Γ_γ[a]	S_γ[a]	$t_1 \sim t_2$(ks)[b]	α_x[b]	χ^2/dof[b]	β_x[b]	S_x[c]	N_H[b]	z[d]
050721	98.4	1.85±0.19	3.62±0.32	0.20∼257.24	1.24±0.02	168/131	$1.43^{+0.33}_{-0.44}$	0.91±0.22	$12.5^{+7.4}_{-12.3}$	...
050922C	4.5	1.37±0.06	1.62±0.05	0.12∼67.53	1.12±0.01	201/142	$1.14^{+0.06}_{-0.08}$	0.67±0.11	$25.0^{+14.9}_{-8.5}$	$2.198^{(1)}$
060111B	58.8	0.96±0.17	1.60±0.14	0.10∼71.70	1.09±0.03	122/84	$1.29^{+0.16}_{-0.18}$	0.25±0.07	$22.0^{+4.7}_{-5.7}$	...
060116	105.9	1.43±0.19	2.41±0.26	0.18∼529.59	1.06±0.03	11/11	$0.89^{+0.17}_{-0.22}$	0.11±0.04	$57.4^{+7.4}_{-14.7}$	$6.6^{(2)}$
060512	8.5	2.49±0.32	0.23±0.04	0.11∼104.01	1.39±0.03	31/31	$0.93^{+0.18}_{-0.18}$	0.53±0.15	< 2.35	$0.4428/2.1^{(3,4)}$
061007	75.3	1.0±0.03	44.41±0.56	0.09∼194.49	1.71±0.01	1667/1133	$0.99^{+0.08}_{-0.08}$	17.78±1.31	$54.4^{+9.6}_{-9.1}$	$1.261^{(5)}$
070318	74.6	1.43±0.09	2.48±0.11	0.07∼943.92	1.11±0.01	359/301	$0.82^{+0.03}_{-0.06}$	1.11±0.16	$56.4^{+3.6}_{-5.4}$	$0.836^{(6)}$
070330	9	2.26±0.27	0.18±0.03	0.08∼167.03	1.01±0.03	62/45	$0.85^{+0.07}_{-0.10}$	0.16±0.06	$6.8^{+3.3}_{-2.2}$	...
070411	121.5	1.76±0.11	2.71±0.16	0.47∼582.08	1.00±0.04	93/54	$1.18^{+0.19}_{-0.09}$	0.47±0.23	$145.8^{+152.5}_{-124.0}$	$2.954^{(7)}$
071020	4.2	1.11±0.05	2.30±0.10	0.07∼632.97	1.03±0.01	458/370	$1.20^{+0.07}_{-0.12}$	0.86±0.12	$13.7^{+1.4}_{-3.1}$	$2.142^{(8)}$
071025	109	1.72±0.06	6.20±0.20	0.15∼316.28	1.47±0.01	467/306	$1.23^{+0.09}_{-0.08}$	4.42±0.65	$8.2^{+1.9}_{-1.9}$	...
080319B	50	1.08±0.02	81.0±1.01	0.07∼174.27	1.58±0.05	1404/978	$0.79^{+0.04}_{-0.04}$	98.82±6.43	$11.1^{+2.7}_{-2.6}$	$0.937^{(9)}$
080413B	8	1.26±0.27	3.20±0.10	0.14∼612.23	0.91±0.01	868/549	$0.90^{+0.05}_{-0.05}$	0.74±0.10	$24.1^{+4.3}_{-4.2}$	$1.1^{(10)}$
080714	33	1.52±0.08	2.50±0.10	0.09∼365.64	1.11±0.02	14/13	$0.61^{+0.18}_{-0.20}$	0.36±0.07	$9.4^{+14.5}_{-9.4}$	...
080804	34	1.19±0.09	3.60±0.20	0.11∼421.02	1.10±0.01	75/101	$0.86^{+0.09}_{-0.06}$	0.42±0.05	$28.2^{+18.9}_{-9.8}$	$2.2045^{(11)}$
080906	147	1.59±0.09	3.50±0.20	0.08∼304.75	1.19±0.01	370/250	$1.05^{+0.07}_{-0.16}$	1.23±0.19	$11.9^{+5.0}_{-4.8}$	$2^{(12)}$
090102	27	1.36±0.08	6.80±0.03	0.39∼688.48	1.35±0.01	196/144	$0.86^{+0.08}_{-0.08}$	3.95±0.61	$64.5^{+14.2}_{-8.6}$	$1.547^{(13)}$
090123	131	1.74±0.12	2.90±0.02	0.11∼183.64	1.51±0.02	213/141	$0.79^{+0.14}_{-0.08}$	1.09±0.24	$0.05^{+2.6}_{-0.1}$	...
090401B	183	1.37±0.05	∼10.0	0.08∼782.30	1.36±0.01	1427/820	$1.02^{+0.10}_{-0.10}$	5.47±0.41	$14.0^{+3.9}_{-2.0}$	...

[a]The power-law photon index and the observed gamma-ray fluence in the BAT band (15-150keV,in units of 10^{-6}erg cm^{-2}).

[b]The time interval for our XRT light curve fitting, and the corresponding temporal decay slope with fitting χ^2/dof, time-integrated spectral index and hydrogen column density N_H at the host galaxy are (in units of 10^{20} cm^{-2}). The spectral parameters are derived from PC data only (from Evens et al. 2008).

[c]The X-ray fluence calculated by integrating the fitting light curve from 10 seconds after the GRB trigger to 10^5 s, in units of 10^{-6}erg cm^{-2}.

[d]The References of redshift.

References. — 1: Jakobsson et al.(2005); 2: Grazian et al.(2006); 3: Bloom et al.(2006b); 4: Starling et al.(2006); 5: Osip et al.(2006); 6: Chen et al.(2007); 7: Jakobsson et al.(2007a); 8: Fatkhullin et al.(2007); 9: Bloom et al.(2008); 10: Cucchiara et al.(2008); 11: Thoene et al.(2008); 12: Hessels et al.(2008); 13: de Ugarte Postigo et al.(2009)

Table 2. The observations and our fits for the GRBs with a canonical XRT lightcurve

GRB	T_{90}(s)	Γ_γ[a]	S_γ[a]	α_1[b]	α_2[b]	χ^2/dof[b]	t_b(ks)[b]	S_X[b]	β_x[c]	N_H[c]	T_0(ks)[d]	χ^2/dof[d]	z	ref[e]
050319	152.5	2.02±0.19	13.10±1.48	0.47±0.36	1.11±0.15	9/11	20.57±9.32	1.34±1.54	$0.95^{+0.07}_{-0.05}$	$9.5^{+23.1}_{-9.5}$	4.93±0.45	110/72	3.24	1
050401	33.3	1.40±0.07	82.20±3.06	0.57±0.02	1.37±0.06	106/92	5.86±0.78	13.21±1.86	$0.99^{+0.11}_{-0.11}$	139^{+65}_{-59}	1.05±0.18	524/330	2.9	2
050416A	2.5	3.08±0.22	3.67±0.37	0.43±0.12	0.90±0.04	36/38	1.74±1.12	1.49±0.35	$1.15^{+0.07}_{-0.05}$	$54.1^{+5.8}_{-7.6}$	0.38±0.08	72/91	0.65	3
050505	58.9	1.41±0.12	24.90±1.79	0.15±0.19	1.30±0.06	26/45	7.87±1.57	3.18±0.56	$1.03^{+0.04}_{-0.05}$	$161.9^{+38.1}_{-21.5}$	7.15±0.41	182/191	4.27	4
050802	19	1.54±0.13	20.0±1.57	0.32±0.10	1.61±0.04	58/72	4.09±0.61	4.82±0.94	$0.89^{+0.03}_{-0.05}$	$2.63^{+0.99}_{-0.96}$	2.22±0.70	185/239	1.71	5
050824	22.6	2.76±0.38	2.66±0.52	0.32±0.06	1.00±0.05	51/39	92.22±49.75	0.93±0.14	$0.93^{+0.14}_{-0.14}$	$3.7^{+8.2}_{-3.7}$	42.41±6.32	51/41	0.83	6
051016B	4	2.40±0.23	1.70±0.22	0.39±0.08	1.18±0.04	15/16	18.77±3.45	2.32±1.01	$1.19^{+0.06}_{-0.13}$	$55.4^{+6.1}_{-14}$	6.34±0.65	53/61	0.94	7
051109A	37.2	1.51±0.20	22.0±2.72	0.79±0.07	1.53±0.08	39/48	27.28±7.90	11.32±4.75	$0.90^{+0.08}_{-0.08}$	$50.8^{+29.6}_{-27.3}$	2.43±0.27	167/167	2.35	8
060115	139.6	1.75±0.12	17.10±1.50	0.61±0.08	1.31±0.11	19/16	37.16±40.16	0.82±0.23	$1.06^{+0.08}_{-0.05}$	< 20.8	11.38±2.07	20/18	3.53	9
060124	8.2	1.84±0.19	4.61±0.53	0.78±0.10	1.65±0.05	165/132	52.65±10.33	30.72±12.36	$1.08^{+0.05}_{-0.05}$	$65.1^{+16}_{-15.2}$	5.57±0.58	337/292	2.297	10
060418	103.1	1.70±0.06	83.30±2.53	0.93±0.07	1.61±0.05	83/76	1.73±1.46	2.16±1.65	$0.89^{+0.10}_{-0.09}$	$34.5^{+16.9}_{-15.6}$	0.45±0.04	84/78	1.49	11
060502A	28.4	1.46±0.08	23.10±1.02	0.53±0.03	1.68±0.15	11/26	72.57±15.05	5.39±1.23	$1.15^{+0.11}_{-0.10}$	$12.5^{+11.7}_{-11.1}$	6.16±0.68	64/70	1.51	12
060714	115	1.93±0.11	28.30±1.67	0.34±0.10	1.27±0.05	53/73	3.70±0.97	2.27±0.52	$1.04^{+0.09}_{-0.08}$	$96.3^{+32.1}_{-29.8}$	1.56±0.15	58/48	2.71	13
060729	115.3	1.75±0.14	26.10±2.11	0.21±0.01	1.42±0.02	459/459	72.97±3.02	20.65±0.89	$1.26^{+0.05}_{-0.05}$	$11.9^{+1.6}_{-1.5}$	51.12±11.21	1246/680	0.54	14
060814	145.3	1.53±0.03	146.0±2.39	0.54±0.02	1.59±0.05	81/57	17.45±1.71	8.02±0.87	$1.30^{+0.07}_{-0.07}$	$28.9^{+2.3}_{-2.2}$	5.34±0.39	228/171	0.84	15
060906	43.5	2.03±0.11	22.10±1.36	0.35±0.10	1.78±0.10	49/32	13.66±3.29	1.18±0.25	$1.12^{+0.13}_{-0.16}$	$245^{+138.6}_{-130.5}$	10.64±1.01	60/34	3.68	16
060908	19.3	1.35±0.06	28.0±1.11	0.70±0.10	1.49±0.08	36/30	0.95±0.34	2.25±1.20	$1.00^{+0.09}_{-0.08}$	$26.2^{+22.2}_{-20}$	0.35±0.03	46/32	2.43	17
060912	5	1.74±0.09	13.50±0.62	0.13±0.30	1.19±0.08	22/28	1.13±0.31	0.92±0.60	$0.95^{+0.11}_{-0.06}$	$24.2^{+8.2}_{-5}$	0.21±0.06	25/30	0.94	18
060927	22.5	1.65±0.08	11.30±0.68	0.60±0.05	1.76±0.20	8/13	3.04±1.41	0.73±0.21	$0.89^{+0.17}_{-0.16}$	$117.7^{+197.5}_{-117.7}$	1.22±0.12	14/16	5.6	19
061121	81.3	1.41±0.03	137.0±1.99	0.75±0.06	1.63±0.05	121/147	24.32±4.38	20.35±5.65	$0.93^{+0.04}_{-0.04}$	$49.2^{+5.5}_{-5.2}$	3.09±0.68	281/285	1.31	20
070306	209.5	1.66±0.10	53.80±2.86	0.12±0.02	1.87±0.03	102/114	29.69±1.72	7.84±0.42	$1.12^{+0.08}_{-0.08}$	$33.4^{+3.1}_{-3}$	29.45±1.26	140/233	1.497	21
070508	20.9	1.35±0.03	196.0±2.73	0.45±0.02	1.42±0.01	516/489	0.77±0.22	19.50±1.53	$0.75^{+0.09}_{-0.09}$	$23.4^{+3.8}_{-3.6}$	0.43±0.02	511/491	0.82	22
070529	109.2	1.34±0.16	25.70±2.45	0.75±0.06	1.32±0.04	30/32	2.25±1.55	1.74±0.31	$0.89^{+0.09}_{-0.10}$	$157.9^{+48.4}_{-62.4}$	0.44±0.06	31/34	2.4996	23
070810A	11	2.04±0.14	6.90±0.60	0.51±0.07	1.31±0.06	24/31	1.72±0.72	1.20±0.26	$1.06^{+0.11}_{-0.10}$	$51.5^{+15.8}_{-19.9}$	0.61±0.08	24/34	2.17	24
071003	150	1.36±0.07	83.0±3.0	-0.20±0.33	1.84±0.04	76/66	30.27±5.16	2.54±0.65	$1.04^{+0.13}_{-0.15}$	$4.8^{+3.2}_{-2.8}$	7.77±1.75	93/68	1.1	25
080210	45	1.77±0.12	18.0±1.0	0.84±0.05	1.47±0.06	45/26	7.04±5.08	2.10±1.06	$1.22^{+0.12}_{-0.10}$	149^{+72}_{-67}	1.02±0.14	35/27	2.64	26
080310	365	2.32±0.16	23.0±2.0	0.27±0.06	1.58±0.04	68/65	10.93±1.17	2.07±0.25	$1.45^{+0.02}_{-0.02}$	70^{+10}_{-10}	7.06±0.62	75/67	2.4266	27
080430	16.2	1.73±0.09	12.0±1.0	0.46±0.02	1.17±0.02	81/140	33.20±6.32	2.73±0.14	$1.05^{+0.07}_{-0.07}$	$33.5^{+4.3}_{-4}$	8.66±0.57	108/142	0.767	28
080516	5.8	1.82±0.27	2.60±0.40	0.29±0.07	1.00±0.06	24/26	2.30±1.17	0.88±0.18	$1.26^{+0.18}_{-0.24}$	$58.3^{+21.8}_{-15.9}$	1.12±0.17	24/29	3.2	29
080605	20	1.11±0.14	133.0±2.0	0.58±0.04	1.43±0.02	359/309	0.60±0.07	15.23±2.52	$0.76^{+0.09}_{-0.08}$	$65.7^{+19.7}_{-18.2}$	0.26±0.01	345/311	1.6398	30
080707	27.1	1.77±0.19	5.20±0.60	0.22±0.05	1.07±0.05	21/21	7.80±3.48	0.74±0.25	$1.11^{+0.17}_{-0.18}$	38^{+19}_{-19}	4.37±0.74	25/22	1.23	31
080710	120	1.47±0.23	14.0±2.0	0.94±0.05	1.80±0.17	79/63	21.30±5.55	4.32±1.03	$1.05^{+0.07}_{-0.09}$	$12.5^{+4.9}_{-4.5}$	8.17±0.65	81/64	0.845	32
080721	16.2	1.11±0.08	120.0±10.0	0.80±0.01	1.65±0.01	1534/1371	3.07±0.34	69.07±4.66	$0.81^{+0.03}_{-0.03}$	$62.6^{+13}_{-12.5}$	0.57±0.07	1899/1373	2602	33
080905B	128	1.78±0.15	18.0±2.0	0.11±0.04	1.42±0.02	81/74	2.93±0.72	8.87±0.87	$0.94^{+0.10}_{-0.06}$	238^{+51}_{-43}	2.28±0.13	104/74	2.347	34
081007	10	2.51±0.20	7.10±0.80	0.72±0.02	1.35±0.05	68/61	56.35±21.72	2.41±0.85	$1.14^{+0.12}_{-0.12}$	$50.9^{+8.5}_{-7.3}$	4.19±0.26	105/92	0.5295	35
081008	185.5	1.69±0.07	43.0±2.0	0.82±0.03	1.86±0.08	30/44	15.71±3.59	3.56±0.53	$1.06^{+0.11}_{-0.06}$	24^{+21}_{-12}	4.01±0.27	41/46	1.967	36
081203A	294	1.54±0.06	77.0±3.0	1.13±0.20	2.06±0.33	232/221	11.49±1.97	13.50±3.01	$1.09^{+0.09}_{-0.08}$	54^{+17}_{-15}	0.72±0.34	304/222	2.1	37
081222	24	1.08±0.15	48.0±1.0	0.63±0.07	1.15±0.02	459/385	0.31±0.11	8.59±1.12	$1.06^{+0.07}_{-0.07}$	60^{+20}_{-19}	0.17±0.01	469/386	2.77	38
090418A	56	1.48±0.07	46.0±2.0	0.38±0.02	1.61±0.03	84/108	2.68±0.32	6.67±0.94	$1.09^{+0.09}_{-0.09}$	115^{+19}_{-18}	1.48±0.16	96/109	1.608	39
090423	10.3	0.80±0.50	5.90±0.40	-0.16±0.07	1.43±0.04	25/39	4.35±0.71	1.19±0.16	$0.83^{+0.10}_{-0.10}$	640^{+280}_{-210}	4.12±0.54	64/40	8.1	40
090424	48	1.19±0.15	210.0±0.0	0.53±0.05	1.20±0.10	586/506	1.06±0.25	32.91±2.22	$0.99^{+0.08}_{-0.08}$	$45^{+5.8}_{-5.4}$	0.65±0.32	591/507	0.544	41
090516A	210	1.84±0.11	90.0±6.0	0.75±0.05	1.84±0.04	139/133	16.32±2.73	4.62±1.01	$1.15^{+0.05}_{-0.06}$	203^{+38}_{-30}	1.09±0.26	158/134	4.109	42
090529	>100	2.01±0.30	6.80±1.70	-0.18±0.23	1.13±0.11	3/5	31.33±15.04	0.51±0.33	$1.16^{+0.12}_{-0.09}$	43^{+22}_{-21}	32.16±15.86	4/6	2.625	3
090618	113.2	1.42±0.08	1050±10	0.71±0.01	1.49±0.01	1130/1078	7.89±0.45	41.71±3.03	$1.01^{+0.05}_{-0.05}$	$22.4^{+2.6}_{-2.5}$	1.63±0.45	1450/1079	0.54	44

[a]TThe power-law photon index and the observed gamma-ray fluence in the BAT band (15-150keV,in units of 10^{-7}erg cm^{-2}).

[b]The decay slopes and the break time of the shallow-to-normal transition in the XRT lightcurve derived from a smooth broken power law fit with fitting χ^2/dof. The X-ray fluences in the XRT band (0.3-10 keV) are integrated from 10 seconds post the GRB trigger to 10^5 seconds,in units of 10^{-7}erg cm^{-2}.

[c]The spectral parameters of the absorbed power law model(from Evens et al. 2008). The N_H of the host galaxy are in units of 10^{20} cm^{-2}.

[d]The zero time $|T_0|$ of the prior X-rays with respect to the GRB trigger time derived from a power-law fit (Eq. 2 in the text).

[f]The reference of redshift.

References. — 1: Fynbo et al.(GCN 3136); 2: Fynbo et al.(GCN 3176); 3: Cenko et al.(GCN 3542); 4: Berger et al.(GCN 3368); 5: Fynbo et al.(GCN 3749); 6: Fynbo et al.(GCN 3874); 7: Soderberg et al.(GCN 4186); 8: Quimby et al.(GCN 4221); 9: Piranomonte et al.(GCN 4520); 10: Cenko et al.(GCN 4592); 11: Dupree et al.(GCN 4969); 12: Cucchiara et al.(GCN 5052); 13: Jakobsson et al.(GCN 5320); 14: Thoene et al.(GCN 5373); 15: Thoene et al.(GCN 6663); 16: Vreeswijk et al.(GCN 5535); 17: Rol et al.(GCN 5555); 18: Jakobsson et al.(GCN 5617); 19: Fynbo et al.(GCN 5651); 20: Bloom et al.(GCN 5826); 21: Jaunsen et al.(GCN 6202); 22: Jakobsson et al.(GCN 6398); 23: Chandra et al.(GCN 6740); 24: Thoene et al.(GCN 6741); 25: Perley et al.(GCN 6850); 26: Cucchiara et al.(GCN 7290); 27: Prochaska et al.(GCN 7388); 28: Cucchiara et al.(GCN 7654); 29: Filgas et al.(GCN 7747); 30: Jakobsson et al.(GCN 7832); 31: Fynbo et al.(GCN 7949); 32: Perley et al.(GCN 7962); 33: D'Avanzo et al.(GCN 7997); 34: Vreeswijk et al.(GCN 8191); 35: Berger et al.(GCN 8335); 36: Cucchiara et al.(GCN 8346); 37: Landsman et al.(GCN 8601); 38: Cucchiara et al.(GCN 8713); 39: Chornock et al.(GCN 9151); 40: Fernandez-Soto et al.(GCN 9222); 41: Chornock et al.(GCN 9243); 42: de Ugarte Postigo et al.(GCN 9383); 43: Malesani et al.(GCN 9457); 44: Cenko et al.(GCN 9518);

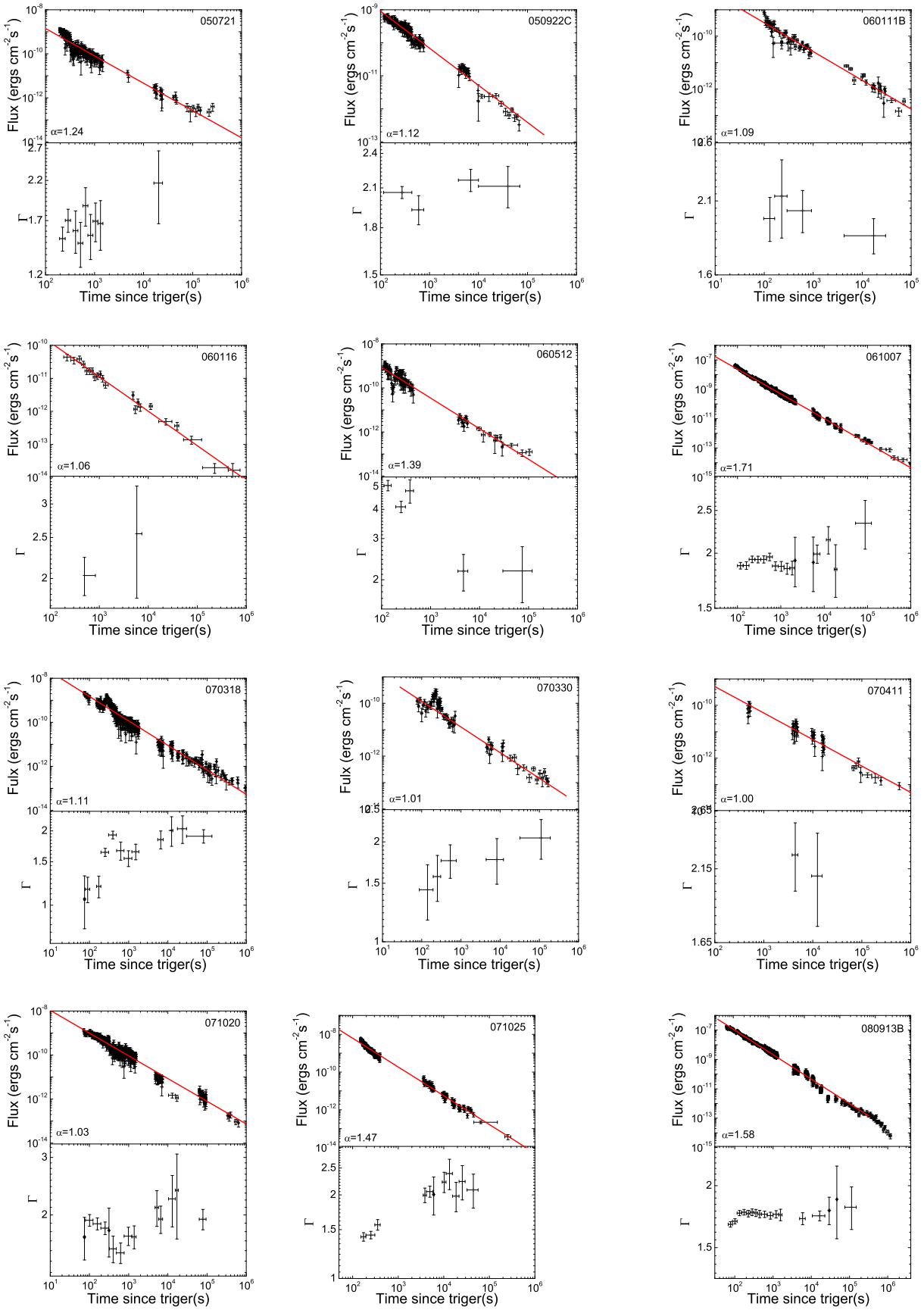

Fig. 1.— XRT lightcurves (top panel) and spectral indices as a function of time (bottom panel) of the 19 GRBs in the SPL sample. The solid lines are the best fits to the SPL model.

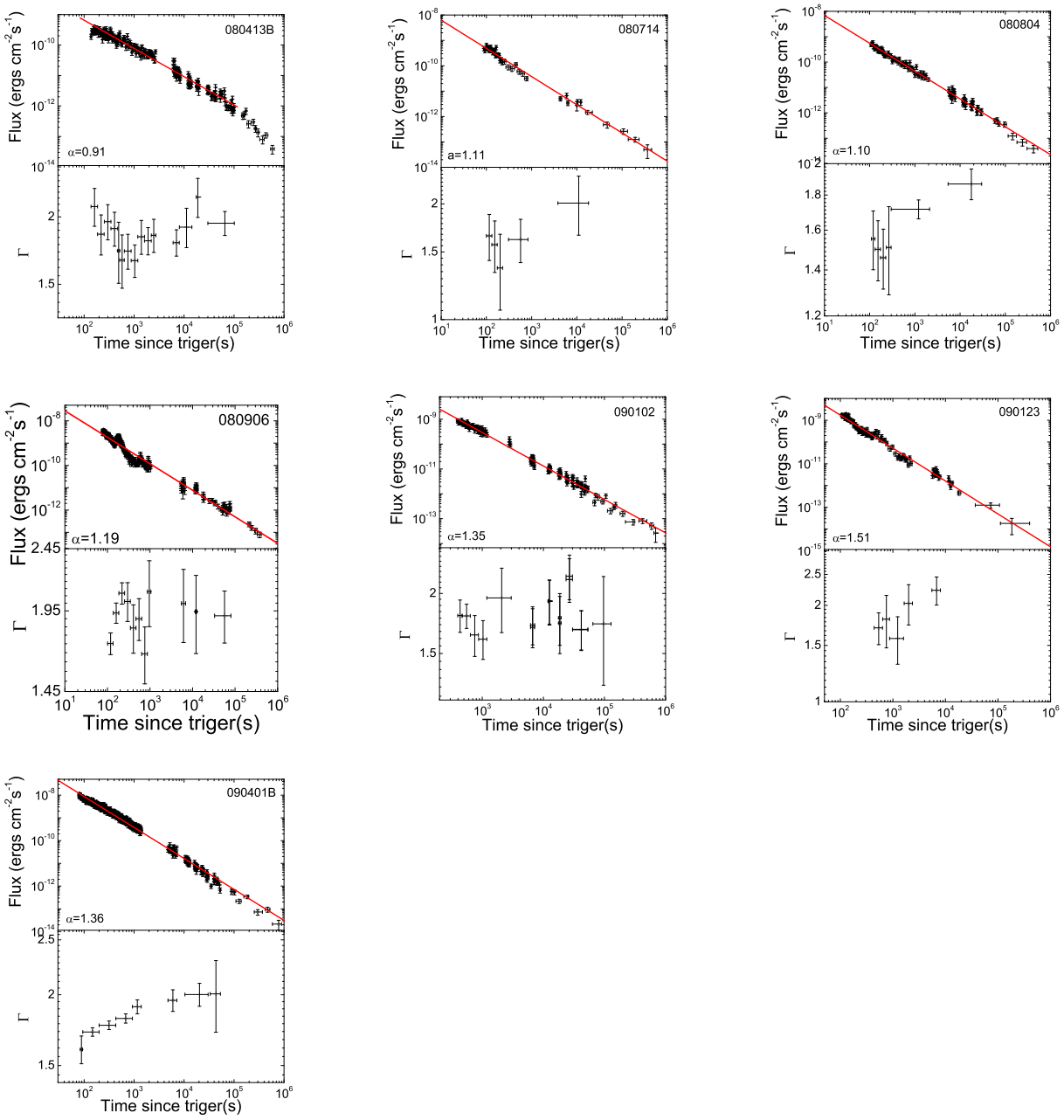

Fig. 1— continued

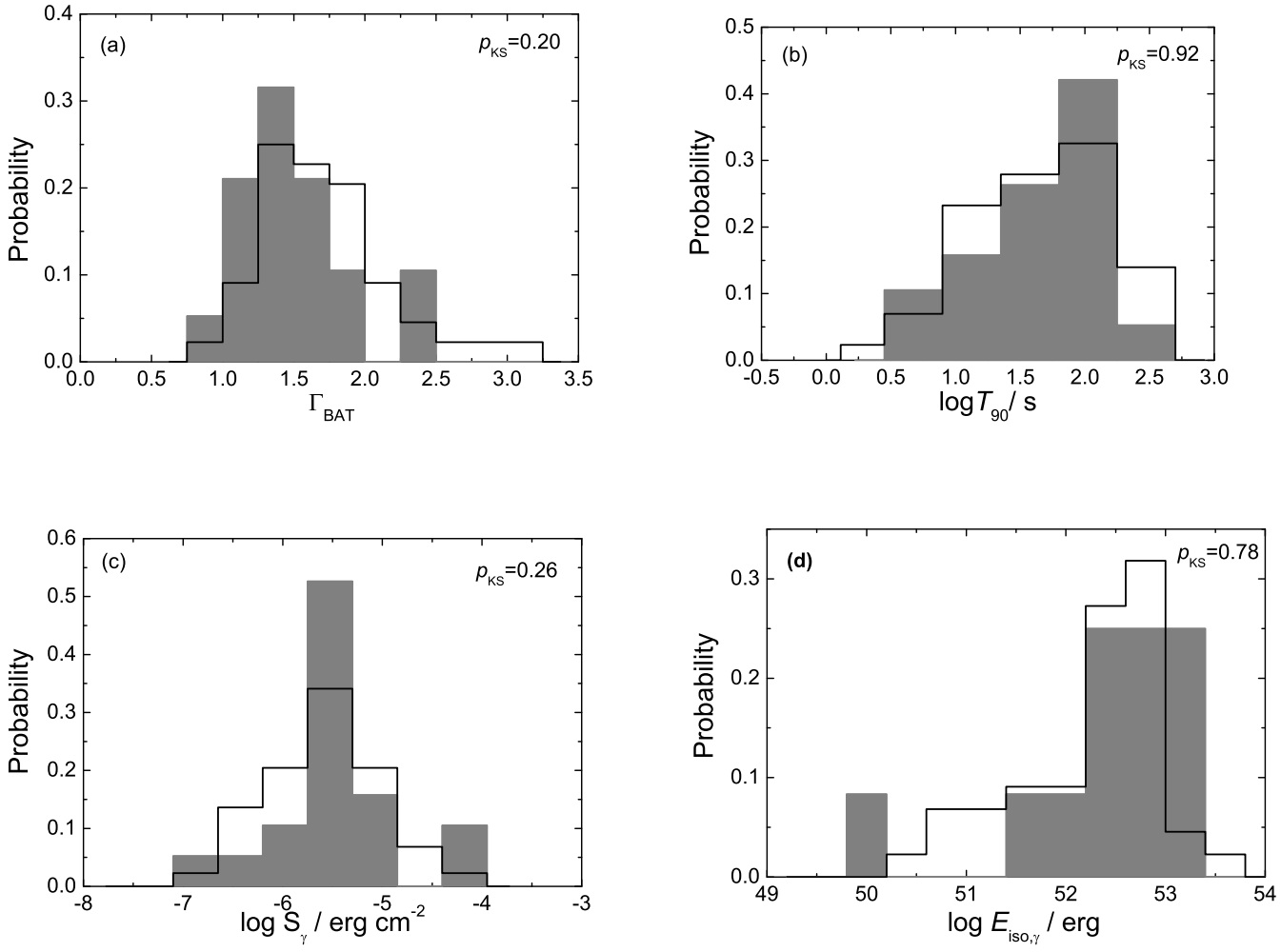

Fig. 2.— Comparisons of the distributions of Γ_{BAT}, T_{90}, S_γ, and $E_{iso,\gamma}$ between the SPL sample (*grey columns*) and the canonical sample (*solid line*). The K-S probability of consistency for each comparison (p_{KS}) is also marked.

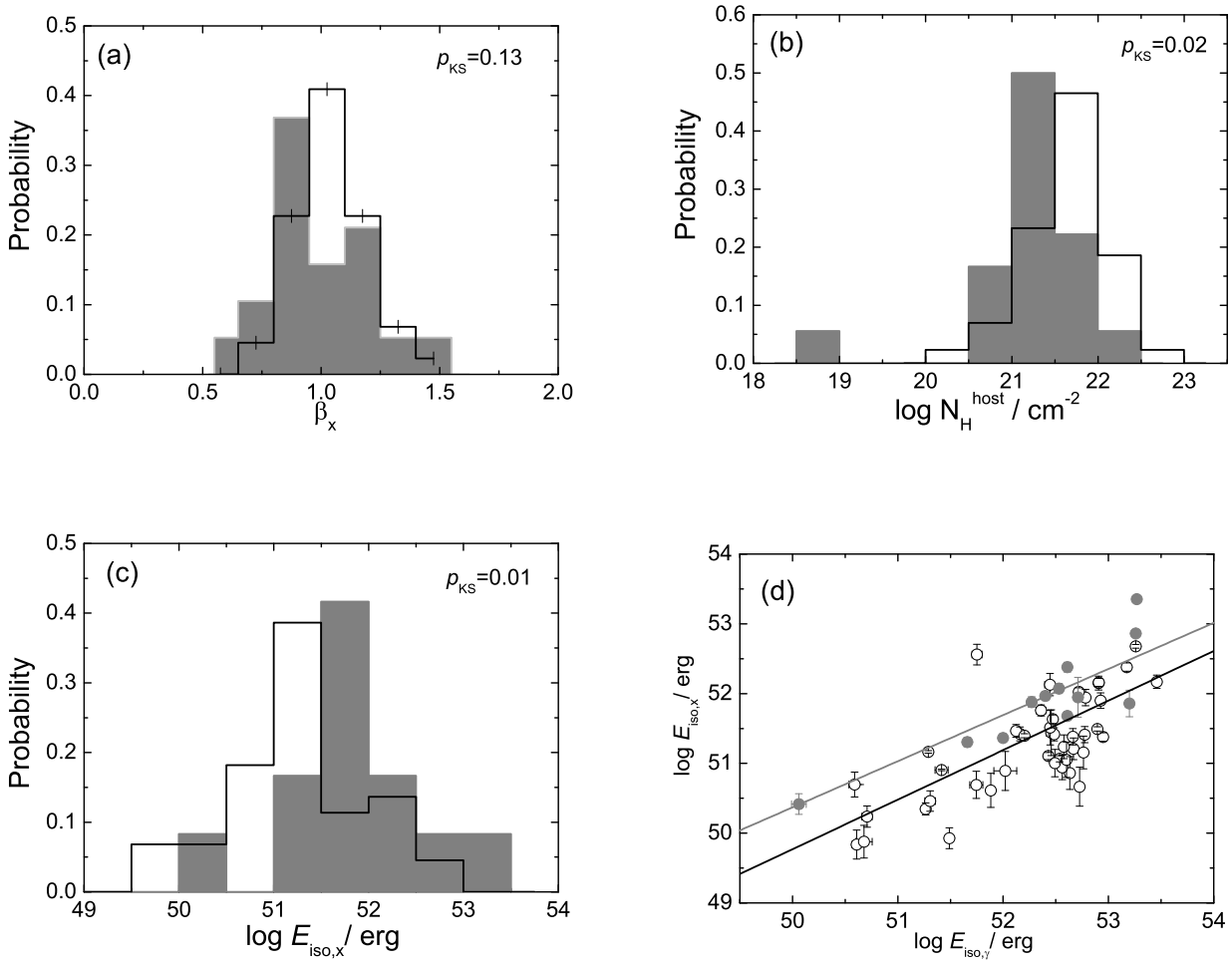

Fig. 3.— Comparisons of the distributions of β_X, N_H and $E_{\rm iso,\ X}$ and the correlations between $E_{\rm iso,\ X}$ and $E_{\rm iso,\ \gamma}$ for the SPL sample (*grey columns or dots*) and the canonical sample (*solid lines or opened dots*)

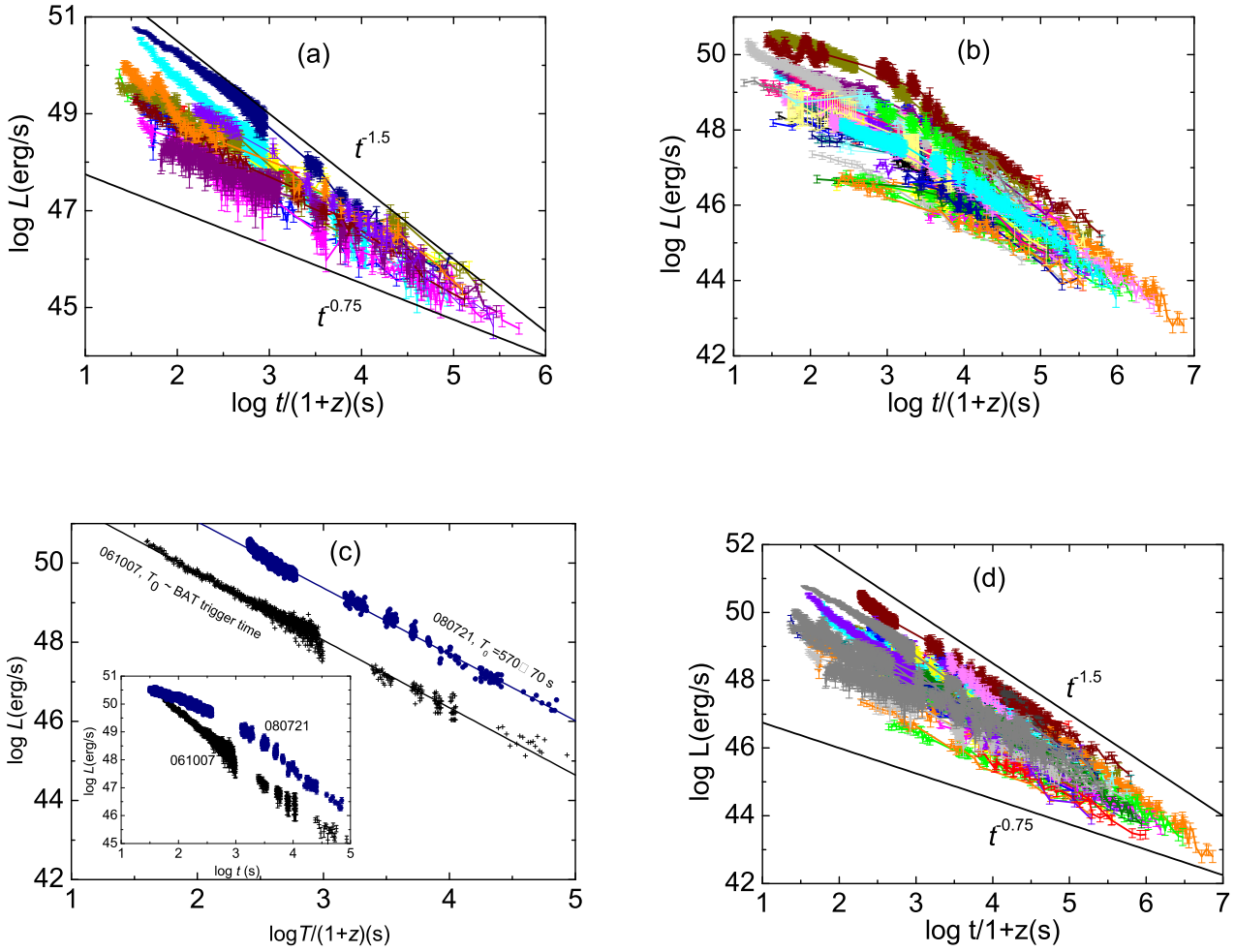

Fig. 4.— X-ray luminosity as a function of time: (a) the observed SPL decay XRT lightcurves referenced to the BAT trigger times; (b) the observed lightcurves of the canonical sample referenced to the BAT trigger time; (c) Illustrations of the XRT lightcurve of GRB 080721 referenced to the T_0 and to the BAT trigger time (inset) with comparisons to the XRT lightcurve of GRB 061007; (d) comparison of the observed SPL lightcurves (grey) referenced to the BAT trigger times and canonical XRT lightcurves referenced to shifted T_0. The decay slopes of the lightcurves predicted by external shock models is $0.75 < \alpha_X < 1.5$, which are shown as solid lines.

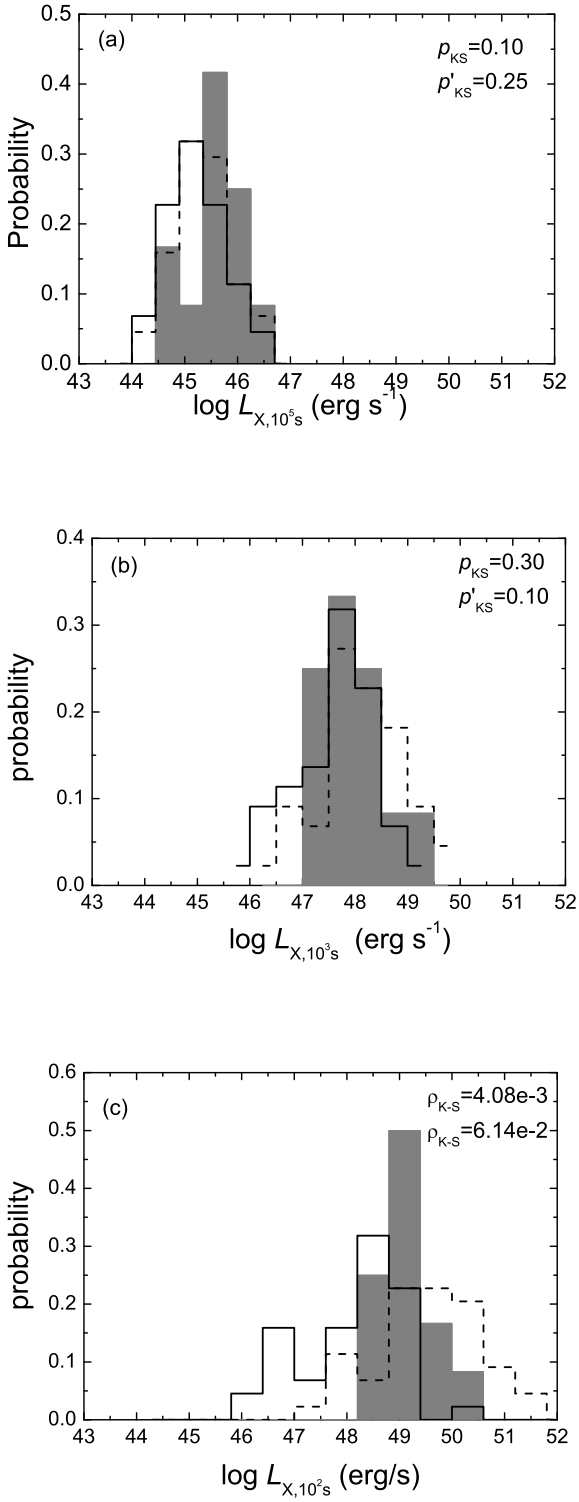

Fig. 5.— Luminosity distributions at 10^5, 10^3, and 10^2 seconds with respect to the BAT trigger times (*solid lines*) and with respect to the T_0's (*solid lines*) for the canonical sample, as compared with the SPL sample (*grey columns*).

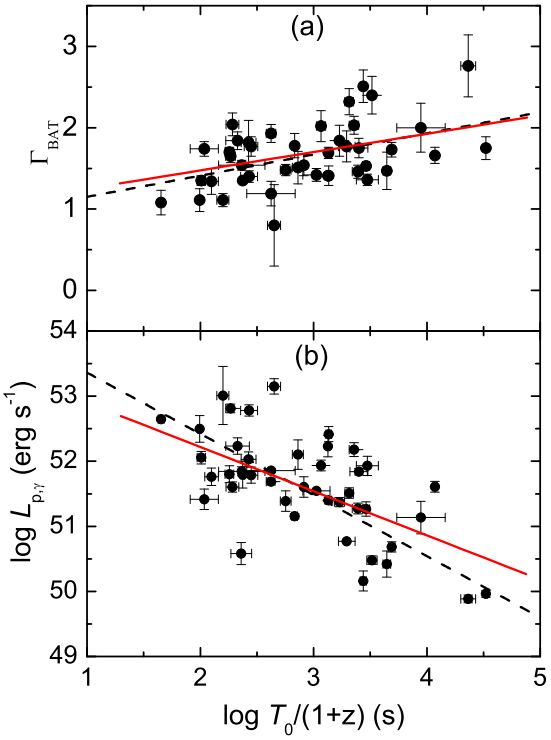

Fig. 6.— Relations of T_0 in the burst frame to the photon index (*panel a*) of prompt gamma-rays and the peak luminosity (*panel b*) for the canonical GRBs in our sample. The dashed and solid lines are the best fit and a robust fit to the data.

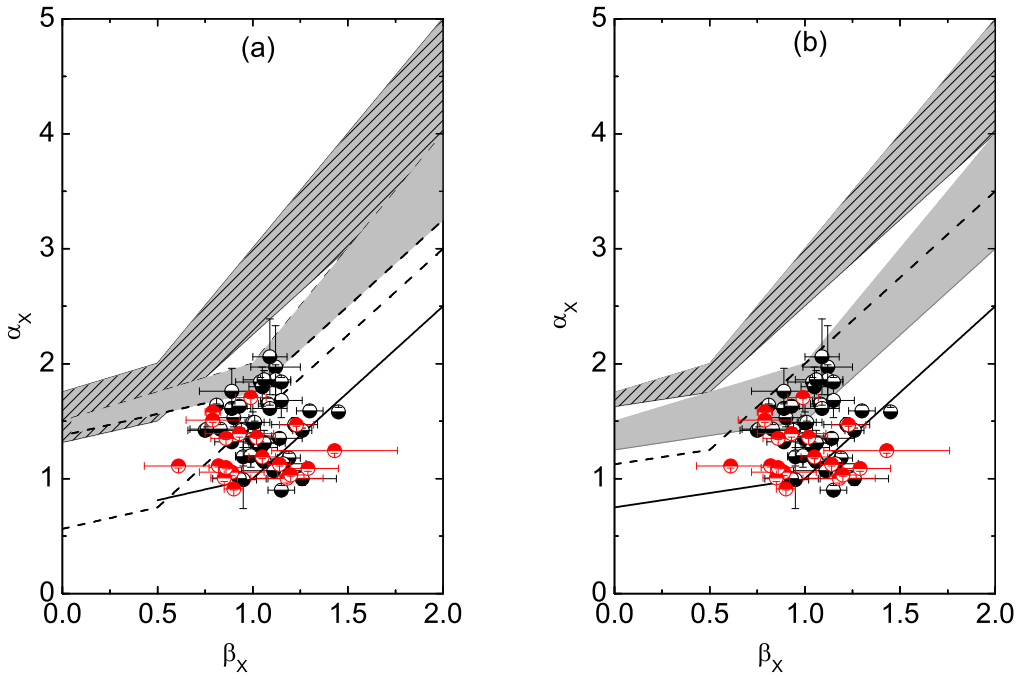

Fig. 7.— Temporal decay index against spectral index for the SPL (*solid dots*) and the T_0-shifted canonical XRT lightcurves (*open circles*). For comparison the closure relations of the external forward shock afterglow models are overplotted. The solid lines and the shaded regions are for the spectral regime I ($\nu_x > \max(\nu_{\rm m}, \nu_{\rm c})$), and the dashed lines and the hatch-shaded regions are for the spectral regime II ($\nu_m < \nu_x < \nu_c$). Panel (a): for an ISM medium; Panel (b): for a wind medium.

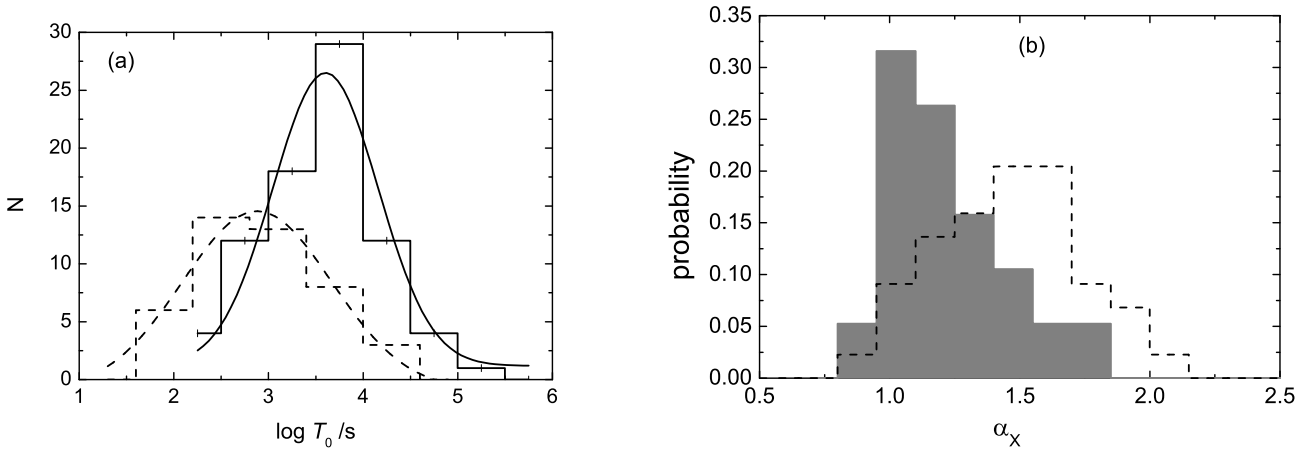

Fig. 8.— *Panel (a)*—Distributions of T_0 in the observed frame for 80 GRBs (*solid line*) and in the burst rest frame for 44 GRBs with redshift measurements (*dashed line*) for the canonical sample. *Panel (b)*—Distribution of the decay slopes of the X-rays with time referenced to T_0 for the 44 GRBs in the canonical sample (*dashed line*) in comparison with the SPL sample (*solid line*).

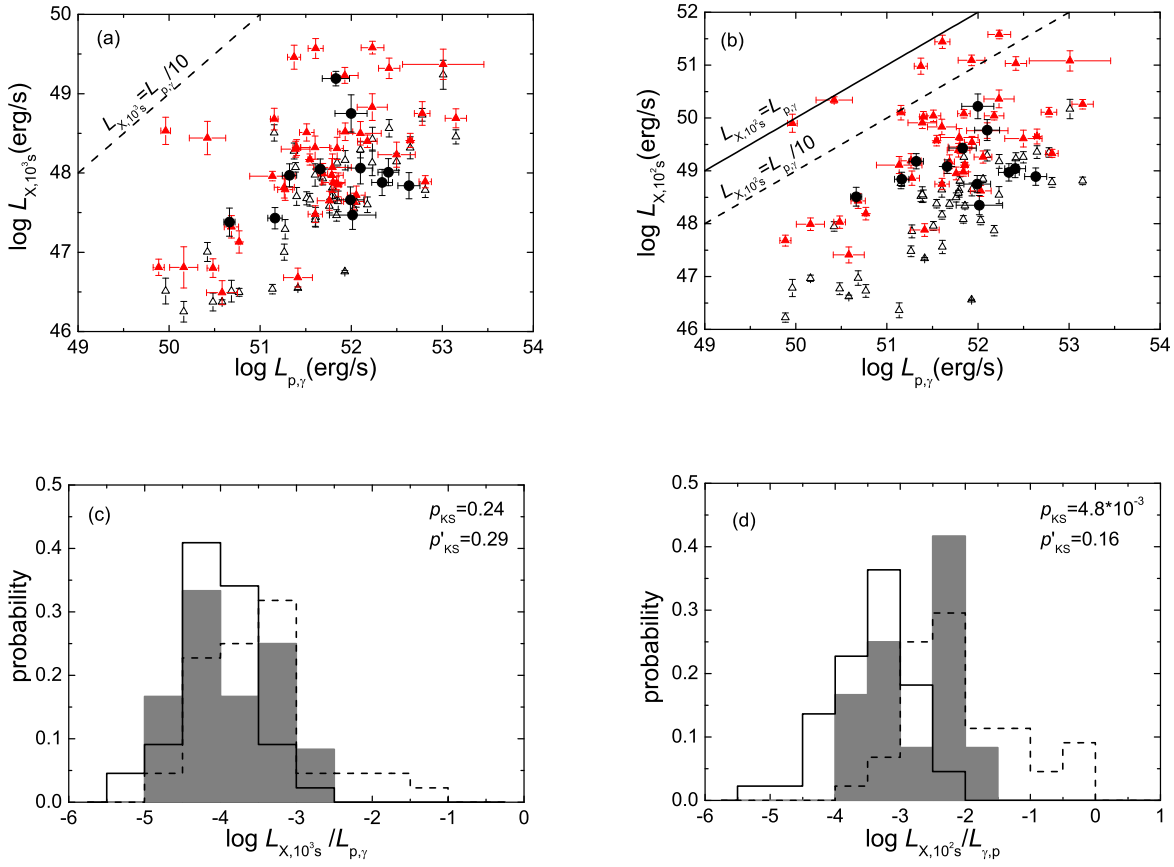

Fig. 9.— *Panels (a) and (b)* — Comparisons of the SPL sample (*solid circles*) with the canonical GRB samples in the ($L_{\rm X,t} - L_{\gamma,p}$)-planes, with $t = 10^2$ seconds and 10^3 seconds referenced to the BAT trigger time (*open triangles*) or to T_0 (*solid triangles*). The lines are $L_{\rm X,t} = L_{\gamma,p}$ and $L_{\rm X,t} = 0.1L_{\gamma,p}$. *Panels (c) and (d)* — Distributions of $\log L_{\rm X}^{\rm BAT}/L_{\gamma,p}$ (*solid line*) and $\log L_X^{T_0}/L_{\gamma,p}$ (*dashed line*) at 10^2 (*panel c*) and 10^3 (*panel d*) seconds for the canonical sample with comparisons to the SPL sample (*grey columns*).